

See discussions, stats, and author profiles for this publication at: <https://www.researchgate.net/publication/343738032>

Displacement-based formulation of Koiter's method: application to multi-modal post-buckling finite element analysis of plates

Preprint · August 2020

DOI: 10.13140/RG.2.2.25893.73441/1

CITATIONS

0

READS

252

2 authors:



Saullo G. P. Castro
Delft University of Technology

67 PUBLICATIONS 678 CITATIONS

[SEE PROFILE](#)



Elco L. Jansen
Hogeschool Rotterdam

194 PUBLICATIONS 797 CITATIONS

[SEE PROFILE](#)

Some of the authors of this publication are also working on these related projects:



Evaluation and modelling of the fatigue damage behaviour of polymer composites at reversed cyclic loading [View project](#)

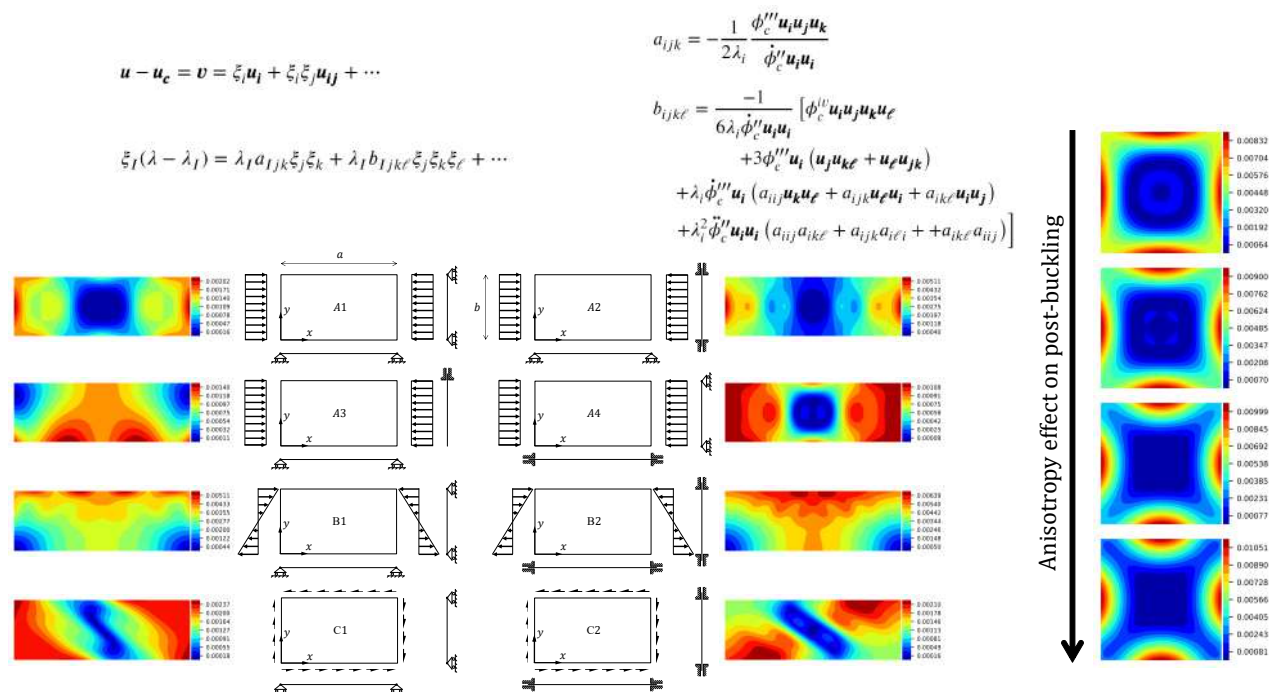


FULLCOMP - FULLY integrated analysis, design, manufacturing and health-monitoring of COMPosite structures [View project](#)

Graphical Abstract

Displacement-based formulation of Koiter's method: application to multi-modal post-buckling finite element analysis of plates

S. G. P. Castro, E. L. Jansen



Highlights

Displacement-based formulation of Koiter's method: application to multi-modal post-buckling finite element analysis of plates

S. G. P. Castro, E. L. Jansen

- Derivation of a complete formulation of Koiter's method for multi-mode analysis
- Achievement of a transparent correspondence between formulation and numerical implementation of Koiter's method
- Application to single-mode and multi-mode initial post-buckling analysis of isotropic and composite plates
- Development of an enhanced Bogner-Fox-Schmit (BFS) finite element with enriched in-plane displacements to verify the formulation
- Verification by comparison with literature
- Calculation and report of reference values for multi-modal expansion coefficients and second-order fields

Displacement-based formulation of Koiter's method: application to multi-modal post-buckling finite element analysis of plates

S. G. P. Castro^a, E. L. Jansen^b

^aDelft University of Technology, Group of Aerospace Structures and Computational Mechanics, Kluyverweg 1 2629 HS Delft, Netherlands

^bRotterdam University of Applied Sciences, School of Engineering and Applied Science, G.J. de Jonghweg 4-6, 3015 GG Rotterdam

ARTICLE INFO

Keywords:

Koiter method
Displacement-based
Buckling
Post-buckling
Finite elements
Classical formulation
Plate

ABSTRACT

Koiter's asymptotic method enables the calculation and deep understanding of the initial post-buckling behaviour of thin-walled structures. For the single-mode asymptotic analysis, Budiansky (1974) presented a clear and general formulation for Koiter's method, based on the expansion of the total potential energy function. The formulation from Budiansky is herein revisited and expanded for the multi-modal asymptotic analysis, of primordial importance in structures with clustered bifurcation modes. Given the admittedly difficult implementation of Koiter's method, especially for multi-modal analysis and during the evaluation of the third- and fourth-order tensors involved in Koiter's analysis; the presented study proposes a formulation and notation with close correspondence with the implemented algorithms. The implementation is based on state-of-the-art collaborative tools: Python, NumPy and Cython. The kinematic relations are specialized using von Kármán shell kinematics, and the displacement field variables are approximated using an enhanced Bogner-Fox-Schmit (BFS) finite element, modified to reach third-order interpolation also for the in-plane displacements, using only 4 nodes per element and 10 degrees-of-freedom per node, aiming an accurate representation of the second-order fields. The formulation and implementation are verified by comparing results for isotropic and composite plates against established literature. Finally, results for multi-modal displacement fields with up to 5 modes and corresponding post-buckling factors are reported for future reference.

1. Introduction

The asymptotic theory originally proposed by Koiter [1] allows a rapid evaluation of the initial post-buckling behavior of structures. The method has been used within a semi-analytical context [2, 3] and has also been applied within a finite element framework [4, 5, 6, 7, 8, 9, 10, 11, 12, 13, 14, 15, 16]. In recent years, the method has been applied in the context of variable stiffness of panel-type structures [17, 18, 14, 16, 19, 20] and in the analysis of imperfection sensitive shells [21, 22, 23].

In particular, the multi-modal formulation of Koiter's approach provides a systematic and efficient procedure to assess the nonlinear behavior of the structure in cases where several buckling modes interact, such as in structures highly optimized for buckling [24, 25, 26] and imperfection-sensitive shell structures [27, 28, 29, 30, 31, 32]. In such designs, small imperfections due to variations in manufacturing parameters can induce different bifurcation paths [33, 34], which can be studied by Koiter's perturbation analysis.

Plates may also show clustered buckling modes, usually when high aspect ratios are involved [16]. Madeo et al. [16] evaluated variable stiffness plates where 4 modes were required in the multi-modal expansion to obtain a satisfactory approximation of the post-buckling behavior. In these studies, the authors used a bi-linear mixed 4-node plate element (MISS-4 [35, 36, 37]) with first-order shear deformation theory.

The aim of the present work is to derive a complete

displacement-based formulation for the single- and multi-modal Koiter's asymptotic analysis. The formulation and notation herein proposed attempts to keep a close correspondence between the theory and the implemented algorithms, and thereby helpful in addressing the issues experienced in the past with the finite element implementation of Koiter's asymptotic method, as highlighted by Casciaro [9].

The following discussion starts revisiting the double expansion of the total potential functional using Koiter's theory, as proposed by Budiansky [38] for a single-mode asymptotic analysis. The formulation is then expanded for the more general case of a multi-modal asymptotic analysis. General-purpose functional derivatives are presented and expressions for these functional derivatives are later obtained using von Kármán non-linear plate kinematics. These expressions can be used with any displacement-based analytical, semi-analytical or numerical approach; and in the present study it is proposed to approximate the displacement fields using the Bogner-Fox-Schmit (BFS) element [39], one of the most accurate rectangular finite elements for predicting the deflection of thin-walled shells, as stated by Zienkiewicz & Taylor [40, p. 153]. The conventional BFS achieves third-order interpolation for the deflection using only 4 nodes per element and 6 degrees-of-freedom per node. An enrichment is proposed to the conventional BFS element to achieve third-order interpolation also for the in-plane displacements, keeping only 4 nodes per element and increasing to 10 degrees-of-freedom per node. This enrichment of the in-plane displacements enable high accuracy while approximating the second-order displacement fields, required in Koiter's method. The developed formulation and implementation is verified against existing literature for

ORCID(s): 0000-0001-9711-0991 (S.G.P. Castro); 0000-0001-7511-2910 (E.L. Jansen)

single- and multi-modal asymptotic expansion of metallic and composite plates, under various loading and boundary conditions. Reference results for multi-modal analysis that are not readily available in the literature are reported, including the second-order displacement fields.

2. Expansion of the Total Potential Energy Functional

Koiter's asymptotic theory was first presented in 1945 [1]. Budiansky [38] presents a complete review of Koiter's asymptotic method, proposing a general-purpose formulation based on the total potential energy functional of the system. The present work elaborates on this formulation and expands it to the complete multi-modal Koiter's analysis. Given a total potential energy functional that has the displacements \mathbf{u} and the a scalar load multiplier λ as unknowns $\phi[\mathbf{u}, \lambda]$. At a pre-buckling static equilibrium:

$$\delta\phi[\mathbf{u}_0, \lambda_0] = \phi'[\mathbf{u}_0, \lambda_0]\delta\mathbf{u} = 0 \quad (1)$$

where \mathbf{u}_0 is a known solution corresponding to the pre-buckling load λ_0 . The formulation herein presented is compatible with either a linear or a nonlinear pre-buckling state. In Eq. 1, the notation $\phi'\delta\mathbf{u}$ is used instead of $\delta\phi$ to conveniently express the functional variation as a tensor product between the Fréchet derivative ϕ' and the variation of the vector containing all degrees-of-freedom $\delta\mathbf{u}$ [38]. The first functional variation becomes a first-order tensor multiplying a vector; the second variation becomes a second-order tensor multiplying two vectors, and so forth, as demonstrated in Eq. 2.

$$\begin{aligned} \delta\phi &= \phi'\delta\mathbf{u} \\ \delta^2\phi &= \phi''\delta\mathbf{u}\delta\mathbf{u} \\ \delta^3\phi &= \phi'''\delta\mathbf{u}\delta\mathbf{u}\delta\mathbf{u} \\ \delta^4\phi &= \phi^{iv}\delta\mathbf{u}\delta\mathbf{u}\delta\mathbf{u}\delta\mathbf{u} \end{aligned} \quad (2)$$

Assume that there exists at least one point of equilibrium that intersects $[\mathbf{u}(\lambda), \lambda]$ at a bifurcation point $[\mathbf{u}_c, \lambda_c]$, such that $\mathbf{u}_c = \lambda_c\mathbf{u}_0$. This bifurcation point is evaluated according to Appendix A. Hence, at the bifurcation point, the following static equilibrium ought to exist:

$$\delta\phi[\mathbf{u}_c, \lambda_c] = \phi'[\mathbf{u}_c, \lambda_c]\delta\mathbf{u} = 0 \quad (3)$$

Assuming that ϕ is continuous at the vicinity of \mathbf{u}_c , a Taylor expansion around the equilibrium point $[\mathbf{u}_c, \lambda_c]$ can be applied on Eq. 3 to find approximations for new state of equilibrium $[\mathbf{u}(\lambda), \lambda], \forall \lambda > \lambda_c$. The error of this approximation becomes zero when $\lim_{\lambda \rightarrow \lambda_c}$. For this first Taylor expansion, a displacement perturbation \mathbf{v} is assumed such that:

$$\mathbf{v} = \mathbf{u}(\lambda) - \mathbf{u}_c \quad (4)$$

with $\lim_{\lambda \rightarrow \lambda_c} \mathbf{v} = \mathbf{0}$ because \mathbf{u} crosses the bifurcation point. The notation $\phi_c^{(n)} = \phi^{(n)}[\mathbf{u}_c, \lambda_c]$, is adopted to obtain the result of the first Taylor expansion shown in Eq. 5, that approximates the total potential energy functional at $[\mathbf{u}, \lambda_c]$, with the new displacement state being $\mathbf{u} = \mathbf{u}_c + \mathbf{v}$.

$$\begin{aligned} \phi'[\mathbf{u}, \lambda_c]\delta\mathbf{u} &= \phi'_c\delta\mathbf{u} + \phi''_c\delta\mathbf{u}\mathbf{v} + \frac{1}{2}\phi'''_c\delta\mathbf{u}\mathbf{v}^2 \\ &\quad + \frac{1}{6}\phi^{iv}_c\delta\mathbf{u}\mathbf{v}^3 + O(4) = 0 \end{aligned} \quad (5)$$

It is worth emphasizing that each Fréchet derivatives from the first expansion of Eq. 5 is calculated at $[\mathbf{u}_c, \lambda_c]$, and not $[\mathbf{u}_0, \lambda_c]$; where $\mathbf{u}_c = \lambda_c\mathbf{u}_0$ and \mathbf{u}_0 is a linear or nonlinear pre-buckling state. Terms $\phi_c^{(n)}$ represent n^{th} -order Fréchet derivatives of the total potential energy functional about the displacement degrees of freedom \mathbf{u} . Equation 2 demonstrates how these Fréchet derivatives of the total potential energy functional ultimately generate n^{th} -order tensors. Vectors $\delta\mathbf{u}$ and \mathbf{v} are 1^{st} -order tensors, such that $\phi_c^{(n)}\mathbf{v}^{(n-1)}\delta\mathbf{u}$ should be read as n^{th} -order tensor products. Defining the following notation for the derivatives of ϕ in terms of λ [38]:

$$\begin{aligned} \phi_c^{(n)} &= \phi^{(n)}[\mathbf{u}_c, \lambda_c] \\ \dot{\phi}_c^{(n)} &= \frac{d}{d\lambda}\phi_c^{(n)} \\ \ddot{\phi}_c^{(n)} &= \frac{d^2}{d\lambda^2}\phi_c^{(n)} \end{aligned} \quad (6)$$

To approximate the total potential energy functional at $[\mathbf{u}, \lambda]$ each Fréchet derivate of Eq. 5 undergoes a second Taylor expansion that assumes $\mathbf{u}(\lambda)$ continuous for any load increment $\lambda - \lambda_c$, resulting in:

$$\phi^{(n)}[\mathbf{u}_c, \lambda] = \phi_c^{(n)} + \dot{\phi}_c^{(n)}(\lambda - \lambda_c) + \frac{1}{2}\ddot{\phi}_c^{(n)}(\lambda - \lambda_c)^2 + O(3) \quad (7)$$

The expressions in Eq. 7 are readily applied into Eq. 5 to obtain the approximation for the total potential energy functional at the new equilibrium, i.e. $\phi'[\mathbf{u}, \lambda]$, which becomes:

$$\begin{aligned} \phi'[\mathbf{u}, \lambda]\delta\mathbf{u} &= \left(\phi''_c + \dot{\phi}''_c(\lambda - \lambda_c) + \frac{1}{2}\ddot{\phi}''_c(\lambda - \lambda_c)^2 + \dots \right) \mathbf{v}\delta\mathbf{u} \\ &\quad + \frac{1}{2} \left(\phi'''_c + \dot{\phi}'''_c(\lambda - \lambda_c) + \frac{1}{2}\ddot{\phi}'''_c(\lambda - \lambda_c)^2 + \dots \right) \mathbf{v}^2\delta\mathbf{u} \\ &\quad + \frac{1}{6} \left(\phi^{iv}_c + \dot{\phi}^{iv}_c(\lambda - \lambda_c) + \frac{1}{2}\ddot{\phi}^{iv}_c(\lambda - \lambda_c)^2 + \dots \right) \mathbf{v}^3\delta\mathbf{u} \\ &\quad + \dots \end{aligned} \quad (8)$$

3. Single-Mode Asymptotic Analysis

Koiter [1] proposed to express $\mathbf{u} - \mathbf{u}_c$ and $\lambda - \lambda_c$ using the following asymptotic expansion:

$$\begin{aligned} \mathbf{u} - \mathbf{u}_c &= \mathbf{v} = \xi\mathbf{u}_I + \xi^2\mathbf{u}_{II} + \xi^3\mathbf{u}_{III} + \dots \\ \lambda - \lambda_c &= a_I\lambda_c\xi + b_I\lambda_c\xi^2 + \dots \end{aligned} \quad (9)$$

where: (1) ξ is a scalar parameter. (2) \mathbf{u}_I is a first-order field, taken directly from one or a linear combination of multiple linear buckling modes. Vector \mathbf{u}_I is customarily re-scaled dividing by the maximum normal displacement amplitude and multiplying by the plate or shell thickness. (3) \mathbf{u}_{II} is a second-order field that provides a correction to the first-order field. (4) The third-order field \mathbf{u}_{III} , and higher, are assumed to have a negligible contribution. (5) a_I and b_I are respectively first- and second-order load parameters to be determined. Equation 9 is a reduced-order model (ROM) relating the load λ and displacement \mathbf{u} around the equilibrium point $[\mathbf{u}_c, \lambda_c]$. Note that this ROM could have been built around any equilibrium point, a property that is explored in the Koiter-Newton approach [41, 42, 43, 44]. Koiter's expansion given by Eq. 9 is directly used into Eq. 8 to render:

$$\begin{aligned} & \xi^2 \left(\frac{1}{2} \mathbf{u}_I^2 \phi_c''' + \mathbf{u}_{II} \phi_c'' + a_I \lambda_c \mathbf{u}_I \dot{\phi}_c'' \right) \delta \mathbf{u} \\ & + \xi^3 \left(\frac{1}{6} \mathbf{u}_I^3 \phi_c^{iv} + a_I \lambda_c \mathbf{u}_{II} \dot{\phi}_c'' + \frac{1}{2} a_I \lambda_c \mathbf{u}_I^2 \phi_c''' \right. \\ & \left. + \frac{1}{2} a_I^2 \lambda_c^2 \mathbf{u}_I \ddot{\phi}_c'' + \mathbf{u}_{III} \phi_c''' + \mathbf{u}_I \mathbf{u}_{II} \phi_c''' + b_I \lambda_c \mathbf{u}_I \dot{\phi}_c'' \right) \delta \mathbf{u} \\ & + \dots = 0 \end{aligned} \quad (10)$$

Note in Eq. 10 that only the terms up to ξ^3 are shown. Equation 10 must be satisfied regardless the values of ξ and $\delta \mathbf{u}$, such that each term must vanish separately. The arbitrary value $\delta \mathbf{u} = \mathbf{u}_I$ can be used [38], with \mathbf{u}_I being the first eigenvector when $I = 1$, or a composition of eigenvectors obtained at the bifurcation point $[\mathbf{u}_c, \lambda_c]$. With $\delta \mathbf{u} = \mathbf{u}_I$ the orthogonality of the second-order field leads to $\dot{\phi}_c'' \mathbf{u}_I \mathbf{u}_{II} = 0$. Hence, Eq. 10 can be used to obtain the equations for a_I and b_I in the single-mode expansion:

$$\begin{aligned} a_I &= -\frac{1}{2\lambda_c} \frac{\mathbf{u}_I^3 \phi_c'''}{\mathbf{u}_I^2 \dot{\phi}_c''} \\ b_I &= -\left(\frac{1}{6} \mathbf{u}_I^4 \phi_c^{iv} + \frac{1}{2} a_I \lambda_c \mathbf{u}_I^3 \dot{\phi}_c''' \right. \\ & \left. + \frac{1}{2} a_I^2 \lambda_c^2 \mathbf{u}_I^2 \ddot{\phi}_c'' + \mathbf{u}_I^2 \mathbf{u}_{II} \phi_c''' \right) / \left(\lambda_c \mathbf{u}_I^2 \dot{\phi}_c'' \right) \end{aligned} \quad (11)$$

Equation 11 is in agreement with Casciaro [9]. Note in Eq. 11 that a_I can be calculated using only \mathbf{u}_I , whereas b_I additionally needs the second-order field \mathbf{u}_{II} . Budiansky [38] suggests to compute \mathbf{u}_{II} using the terms for ξ^2 in Eq. 10:

$$\phi_c'' \bar{\mathbf{u}}_{II} \delta \mathbf{u} + \frac{1}{2} \mathbf{u}_I^2 \phi_c''' \delta \mathbf{u} + a_I \lambda_c \mathbf{u}_I \dot{\phi}_c'' \delta \mathbf{u} = 0$$

which must hold for all arbitrary variations $\delta \mathbf{u}$, such that:

$$\phi_c'' \bar{\mathbf{u}}_{II} + \frac{1}{2} \mathbf{u}_I^2 \phi_c''' + a_I \lambda_c \mathbf{u}_I \dot{\phi}_c'' = 0 \quad (12)$$

For problems in solid mechanics ϕ_c'' will generally be an invertible positive-definite square matrix [38], such that the solution of Eq. 12 can be:

$$\bar{\mathbf{u}}_{II} = [\phi_c'']^{-1} \left(-\frac{1}{2} \phi_c''' \mathbf{u}_I^2 - a_I \lambda_c \mathbf{u}_I \dot{\phi}_c'' \right) \quad (13)$$

Note in Eqs. 12 and 13 that vector $\bar{\mathbf{u}}_{II}$ is appropriately used instead of \mathbf{u}_{II} because Eq. 13 allows multiple solutions of $\bar{\mathbf{u}}_{II}$ for different multipliers applied to \mathbf{u}_I . However, one must guarantee that any calculated $\bar{\mathbf{u}}_{II}$ is orthogonal to \mathbf{u}_I such that the second-order displacement vector \mathbf{u}_{II} becomes a valid vector basis for the reduced-order model of Eq. 9. Gram-Schmidt orthogonalization [45] can be used to obtain the orthogonal component of $\bar{\mathbf{u}}_{II}$, where first the projection of $\bar{\mathbf{u}}_{II}$ onto \mathbf{u}_I is obtained as:

$$proj_{\mathbf{u}_I} \bar{\mathbf{u}}_{II} = \mathbf{u}_I \frac{\langle \bar{\mathbf{u}}_{II}, \mathbf{u}_I \rangle}{\langle \mathbf{u}_I, \mathbf{u}_I \rangle}$$

Next, the orthogonal \mathbf{u}_{II} can be calculated subtracting the projection from $\bar{\mathbf{u}}_{II}$, using:

$$\mathbf{u}_{II} = \bar{\mathbf{u}}_{II} - \mathbf{u}_I \frac{\langle \bar{\mathbf{u}}_{II}, \mathbf{u}_I \rangle}{\langle \mathbf{u}_I, \mathbf{u}_I \rangle} \quad (14)$$

4. Multi-Modal Asymptotic Analysis

The possibility to perform post-buckling analysis in structures with clustered buckling modes is one of the apparent advantages of Koiter's method compared to other methods [9, 16]. The necessity of considering multiple modes in the asymptotic expansion has been demonstrated by many authors, e.g. when the vibration frequencies are closely spaced [46]; variable-angle tow plates with clustered buckling modes [16]; and imperfection sensitive structures [47, 38, 48, 28, 49, 29, 50, 22].

The single-mode asymptotic expansion of Eq. 9 can be generalized to a multi-modal asymptotic expansion, as shown in Eqs. 15 and 16 [51, 12]:

$$\mathbf{u} - \mathbf{u}_c = \mathbf{v} = \xi_i \mathbf{u}_i + \xi_i \xi_j \mathbf{u}_{ij} + \dots \quad (15)$$

$$\xi_I (\lambda - \lambda_I) = \lambda_I a_{Ijk} \xi_j \xi_k + \lambda_I b_{Ijk\ell} \xi_j \xi_k \xi_\ell + \dots \quad (16)$$

where summation convention is applied for repeated indices $j, k, \ell = 1, 2, \dots, m$ is applied. Equation 16 is a reduced-order model consisting of a system of m equations obtained for $I = 1, 2, \dots, m$, which has $\xi_1, \xi_2, \dots, \xi_m$ unknowns. The value λ_I correspond to the I^{th} linear buckling eigenvalue \mathbf{u}_I , always re-scaled by dividing with the

maximum out-of-plane displacement and multiplying by the plate thickness. Finding the right number of linear buckling modes m in the multi-modal analysis is a common question [9], and an accepted criterion is to select a number of modes that lies within 10%-20% departing from the first critical load [9].

Note that Eq. 15 consists on a reduced-order model to calculate displacements \mathbf{u} based on a pre-buckled state \mathbf{u}_c with known linear buckling modes \mathbf{u}_i and known second-order displacement fields \mathbf{u}_{ij} . As in the case of the single-mode expansion, for plates and shells it is customary to re-scale \mathbf{u}_{ij} dividing by the maximum normal displacement amplitude of \mathbf{u}_{ij} and multiplying by the plate or shell thickness. The coefficients ξ_i for $i = 1, \dots, m$ are found for each load λ after solving the system of m equations given by Eq. 16. Solving Eq. 16 requires the calculation of all coefficients a_{ijk} and b_{ijkl} .

The expressions given by Eqs. 15 and 16 are applied to the expanded total potential energy functional of Eq. 8. The terms multiplying $\xi_j \xi_k$ and $\xi_j \xi_k \xi_\ell$ are collected, analogously to the terms multiplying ξ^2 and ξ^3 for the single-mode expansion in Eq. 10. The collected terms for the multi-modal expansion are shown in Eq. 17, where the following orthogonality property of the linear buckling modes is used: $\langle \mathbf{u}_i, \mathbf{u}_j \rangle = 0, \forall i \neq j$; leading to $\phi_c'' \mathbf{u}_i \mathbf{u}_j = 0, \forall i \neq j$; $\dot{\phi}_c'' \mathbf{u}_i \mathbf{u}_j = 0, \forall i \neq j$; and $\ddot{\phi}_c'' \mathbf{u}_i \mathbf{u}_j = 0, \forall i \neq j$. Moreover, collected terms in brackets that are multiplying any of the perturbation parameters $\xi_{j,k,\ell}$ ultimately vanish, knowing that $\xi_{j,k,\ell} \rightarrow 0$.

$$\begin{aligned} & \xi_j \xi_k \left[(a_{ijk} + a_{ikj}) \lambda_i \mathbf{u}_i \dot{\phi}_c'' + \phi_c''' \mathbf{u}_j \mathbf{u}_k + \phi_c'' \mathbf{u}_{jk} + \phi_c'' \mathbf{u}_{kj} \right] \delta \mathbf{u} \\ & + \xi_j \xi_k \xi_\ell \left[\lambda_i \dot{\phi}_c'' \mathbf{u}_i (b_{ijkl} + b_{iklj} + b_{ilkj} \right. \\ & \quad \left. + b_{ijlk} + b_{ikjl} + b_{iljk}) + \phi_c^{iv} \mathbf{u}_j \mathbf{u}_k \mathbf{u}_\ell \right. \\ & \quad \left. + \phi_c''' (\mathbf{u}_j \mathbf{u}_{k\ell} + \mathbf{u}_j \mathbf{u}_{\ell k} + \mathbf{u}_k \mathbf{u}_{j\ell} \right. \\ & \quad \left. + \mathbf{u}_k \mathbf{u}_{\ell j} + \mathbf{u}_\ell \mathbf{u}_{jk} + \mathbf{u}_\ell \mathbf{u}_{kj}) \right. \\ & \quad \left. + \ddot{\phi}_c'' \lambda_i^2 \mathbf{u}_i (a_{ijl} a_{ik\ell} + a_{iji} a_{ik\ell} + a_{iji} a_{i\ell k} + a_{iji} a_{i\ell k} \right. \\ & \quad \left. + a_{iik} a_{ij\ell} + a_{iki} a_{ij\ell} + a_{iik} a_{i\ell j} + a_{iki} a_{i\ell j} \right. \\ & \quad \left. + a_{i\ell l} a_{ijk} + a_{i\ell i} a_{ijk} + a_{i\ell l} a_{ikj} + a_{i\ell i} a_{ikj}) \right. \\ & \quad \left. + \dot{\phi}_c''' \lambda_i (a_{iji} \mathbf{u}_k \mathbf{u}_\ell + a_{iji} \mathbf{u}_k \mathbf{u}_\ell + a_{iik} \mathbf{u}_j \mathbf{u}_\ell + a_{iki} \mathbf{u}_j \mathbf{u}_\ell \right. \\ & \quad \left. + a_{iil} \mathbf{u}_j \mathbf{u}_k + a_{i\ell i} \mathbf{u}_j \mathbf{u}_k + a_{ijk} \mathbf{u}_i \mathbf{u}_\ell + a_{ikj} \mathbf{u}_i \mathbf{u}_\ell \right. \\ & \quad \left. + a_{ij\ell} \mathbf{u}_i \mathbf{u}_k + a_{i\ell j} \mathbf{u}_i \mathbf{u}_k + a_{ik\ell} \mathbf{u}_i \mathbf{u}_j + a_{i\ell k} \mathbf{u}_i \mathbf{u}_j) \right] \delta \mathbf{u} \\ & + \dots = 0 \end{aligned} \quad (17)$$

For the expanded equilibrium to be stationary, each term in Eq. 17 must vanish separately, similarly to the single-mode expansion. Assuming $\delta \mathbf{u} = \mathbf{u}_i$ in Eq. 17, the expressions for a_{ijk} and b_{ijkl} can be obtained, as respectively given

in Eqs. 18 and 19.

$$a_{ijk} = -\frac{1}{2\lambda_i} \frac{\phi_c''' \mathbf{u}_i \mathbf{u}_j \mathbf{u}_k}{\dot{\phi}_c'' \mathbf{u}_i \mathbf{u}_i} \quad (18)$$

$$\begin{aligned} b_{ijkl} = & \frac{-1}{6\lambda_i \phi_c'' \mathbf{u}_i \mathbf{u}_i} [\phi_c^{iv} \mathbf{u}_i \mathbf{u}_j \mathbf{u}_k \mathbf{u}_\ell \\ & + 3\phi_c''' \mathbf{u}_i (\mathbf{u}_j \mathbf{u}_{k\ell} + \mathbf{u}_\ell \mathbf{u}_{jk}) \\ & + \lambda_i \dot{\phi}_c'' \mathbf{u}_i (a_{iji} \mathbf{u}_k \mathbf{u}_\ell + a_{ijk} \mathbf{u}_\ell \mathbf{u}_i + a_{ikl} \mathbf{u}_i \mathbf{u}_j) \\ & + \lambda_i^2 \ddot{\phi}_c'' \mathbf{u}_i \mathbf{u}_i (a_{iji} a_{ik\ell} + a_{ijk} a_{i\ell i} + a_{ikl} a_{iij})] \end{aligned} \quad (19)$$

Note in the calculation of b_{ijkl} that the second-order fields \mathbf{u}_{ij} are needed. As in the single-mode expansion case, a non-orthogonal second-order field $\bar{\mathbf{u}}_{ij}$ is calculated first. Note that the terms in brackets multiplying $\xi_j \xi_k$ in Eq. 17 are obtained for any i^{th} mode. Therefore, the contribution for all $i = 1, \dots, m$ modes are added and the following equation for $\bar{\mathbf{u}}_{ij}$ is obtained:

$$\bar{\mathbf{u}}_{jk} = [\phi_c''']^{-1} \left(-\frac{1}{2} \phi_c''' \mathbf{u}_j \mathbf{u}_k - \frac{1}{m} \sum_{i=1}^{i=m} a_{ijk} \lambda_i \mathbf{u}_i \dot{\phi}_c'' \right) \quad (20)$$

The orthogonal second-order field vectors in the multi-modal asymptotic expansion can be obtained after successive Gram-Schmidt orthogonalization [45] operations, used to remove the components of $\bar{\mathbf{u}}_{jk}$ that are parallel to all linear buckling modes used in the multi-modal expansion \mathbf{u}_i , with $i = 1, 2, \dots, m$. This orthogonalization procedure is formulated in Eq. 21.

$$\mathbf{u}_{jk} = \bar{\mathbf{u}}_{jk} - \sum_{i=1}^{i=m} \mathbf{u}_i \frac{\langle \bar{\mathbf{u}}_{jk}, \mathbf{u}_i \rangle}{\langle \mathbf{u}_i, \mathbf{u}_i \rangle} \quad (21)$$

5. Functional Derivatives using Von Kármán Kinematics

This section demonstrates how to calculate the functional derivatives leading to the n^{th} -order tensors $\phi_c^{(n)}$, $\dot{\phi}_c^{(n)}$ and $\ddot{\phi}_c^{(n)}$, previously introduced during the single-mode and multi-modal asymptotic expansions. The discussion focus on von Kármán non-linear kinematics, and can be easily extended to other non-linear kinematic equations, such as those proposed by Sanders [49, 52] and Timoshenko & Gere [52, section 2.2.4].

5.1. Strains

Von Kármán proposed a kinematic relation for plates that neglect various non-linear terms that come from the full non-linear Green-Lagrange strain-displacement relations [52, section 2.2.2]. Von Kármán kinematics are also referred to in the literature as Donnell-type [53, 54] or Kirchhoff-Love non-linear equations. Using classical equivalent single

layer theory, the three-dimensional strains are expressed as $\boldsymbol{\epsilon}(x, y, z) = \boldsymbol{\epsilon}(x, y) + z\boldsymbol{\kappa}(x, y)$, such that the extensional $\boldsymbol{\epsilon}$ and rotational $\boldsymbol{\kappa}$ strains can be defined in terms of the in-plane displacement field variables $u(x, y), v(x, y), w(x, y)$ as:

$$\boldsymbol{\epsilon} = \begin{Bmatrix} \epsilon_{xx} \\ \epsilon_{yy} \\ \gamma_{xy} \end{Bmatrix} = \begin{Bmatrix} u_{,x} + \frac{1}{2}w_{,x}^2 \\ v_{,y} + \frac{1}{2}w_{,y}^2 \\ u_{,y} + v_{,x} + w_{,x}w_{,y} \end{Bmatrix} \quad (22)$$

$$\boldsymbol{\kappa} = \begin{Bmatrix} \kappa_{xx} \\ \kappa_{yy} \\ \kappa_{xy} \end{Bmatrix} = \begin{Bmatrix} -w_{,xx} \\ -w_{,yy} \\ -2w_{,xy} \end{Bmatrix}$$

Assuming the following approximation for the displacement field:

$$u, v, w^T = \mathbf{S}^u \mathbf{u}$$

$$\mathbf{S}^u = \begin{Bmatrix} \mathbf{S}^u \\ \mathbf{S}^v \\ \mathbf{S}^w \end{Bmatrix} \quad (23)$$

where $\mathbf{S}^{u,v,w}$ are known shape functions; each component u, v, w can be written adopting summation convention for repeated indices as:

$$\begin{aligned} u &= S_a^u u_a \\ v &= S_a^v u_a \\ w &= S_a^w u_a \end{aligned} \quad (24)$$

with $a = 1, 2, \dots, n$. The strain variations can be represented as:

$$\begin{aligned} \delta\boldsymbol{\epsilon} &= \boldsymbol{\epsilon}' \delta\mathbf{u} \\ \delta\boldsymbol{\kappa} &= \boldsymbol{\kappa}' \delta\mathbf{u} \end{aligned} \quad (25)$$

where the $'$ (prime) symbol is used to denote a Frechét's differentiation. Adopting index notation to represent the strains, such that $\epsilon_1 = \epsilon_{xx}, \epsilon_2 = \epsilon_{yy}, \epsilon_3 = \gamma_{xy}, \kappa_1 = \kappa_{xx}, \kappa_2 = \kappa_{yy}, \kappa_3 = \kappa_{xy}$; the first and second variations of the extensional and rotational strains become:

$$\begin{aligned} \delta\epsilon_i &= \epsilon'_{ia} \delta u_a \\ \delta\kappa_i &= \kappa'_{ia} \delta u_a \\ \delta(\delta\epsilon_i) &= \epsilon''_{iab} \delta u_a \delta u_b \\ \delta(\delta\kappa_i) &= \kappa''_{iab} \delta u_a \delta u_b \end{aligned} \quad (26)$$

With these definitions, the first Frechét's differentiation of the strains can be represented as:

$$\boldsymbol{\epsilon}'_a = \begin{Bmatrix} S_{a,x}^u + w_{,x}S_{a,x}^w \\ S_{a,y}^v + w_{,y}S_{a,y}^w \\ S_{a,y}^u + S_{a,x}^v + w_{,x}S_{a,y}^w + w_{,y}S_{a,x}^w \end{Bmatrix} \quad (27)$$

$$\boldsymbol{\kappa}'_a = \begin{Bmatrix} -S_{a,xx}^w \\ -S_{a,yy}^w \\ -2S_{a,xy}^w \end{Bmatrix}$$

The second differentiation:

$$\boldsymbol{\epsilon}''_{ab} = \begin{Bmatrix} S_{a,x}^w S_{b,x}^w \\ S_{a,y}^w S_{b,y}^w \\ S_{a,y}^w S_{b,x}^w + S_{a,x}^w S_{b,y}^w \end{Bmatrix} \quad (28)$$

$$\boldsymbol{\kappa}''_{ab} = \mathbf{0}$$

Note in Eq. 28 that $\boldsymbol{\epsilon}''_{iab}$ represents a symmetric second-order tensor, which is an important property to be considered while implementing the method.

For the differentiations with respect to λ , we must recall that all functional expansions were calculated about the bifurcation point $[\mathbf{u}_c, \lambda_c]$, such that the strains and stresses are those corresponding to the displacement $\mathbf{u}_c = \lambda \mathbf{u}_0$, with $\lambda = \dot{\lambda}_c$. Starting with $\boldsymbol{\epsilon}$ and $\boldsymbol{\kappa}$, using the notation $\partial(\cdot)/\partial\lambda = (\cdot)$ and $\partial^2(\cdot)/\partial\lambda^2 = (\ddot{\cdot})$:

$$\dot{\boldsymbol{\epsilon}} = \begin{Bmatrix} u_{0,x} + \lambda w_{0,x}^2 \\ v_{0,y} + \lambda w_{0,y}^2 \\ u_{0,y} + v_{0,x} + 2\lambda w_{0,x}w_{0,y} \end{Bmatrix} \quad (29)$$

$$\dot{\boldsymbol{\kappa}} = \begin{Bmatrix} -w_{0,xx} \\ -w_{0,yy} \\ -2w_{0,xy} \end{Bmatrix}$$

If the pre-buckling state \mathbf{u}_0 is evaluated linearly for a plate with no bending-extension coupling and only in-plane pre-buckling loads, $w_0 = 0$ and the initial post-buckling analysis is greatly simplified. Nevertheless, the formulation presented next is valid for the more general case of $w_0 \neq 0$.

The second differentiation with respect to λ gives:

$$\ddot{\boldsymbol{\epsilon}} = \begin{Bmatrix} w_{0,x}^2 \\ w_{0,y}^2 \\ 2w_{0,x}w_{0,y} \end{Bmatrix} \quad (30)$$

$$\ddot{\boldsymbol{\kappa}} = \mathbf{0}$$

For $\boldsymbol{\epsilon}'_a$ and $\boldsymbol{\kappa}'_a$, the first differentiation with respect to λ gives:

$$\dot{\boldsymbol{\epsilon}}'_a = \begin{Bmatrix} w_{0,x}S_{a,x}^w \\ w_{0,y}S_{a,y}^w \\ w_{0,x}S_{a,y}^w + w_{0,y}S_{a,x}^w \end{Bmatrix} \quad (31)$$

$$\dot{\boldsymbol{\kappa}}'_a = \mathbf{0}$$

For the second differentiations with respect to λ , $\ddot{\boldsymbol{\epsilon}}'_a = \mathbf{0}$ and $\ddot{\boldsymbol{\kappa}}'_a = \mathbf{0}$. For $\boldsymbol{\epsilon}''_{ab}$ and $\boldsymbol{\kappa}''_{ab}$ all derivatives with respect to λ are zero.

5.2. Stresses

Based on Eqs. 22 - 31 it is straightforward to compute the corresponding stresses. Using classical constitutive relations for laminated composites [55] and adopting the index notation: $N_1 = N_{xx}$, $N_2 = N_{yy}$ and $N_3 = N_{xy}$; $M_1 = M_{xx}$, $M_2 = M_{yy}$ and $M_3 = M_{xy}$; the stress-strain relations can be written as:

$$\begin{aligned} N_i &= A_{ij}\varepsilon_j + B_{ij}\kappa_j \\ M_i &= B_{ij}\varepsilon_j + D_{ij}\kappa_j \end{aligned} \quad (32)$$

where A_{ij} represents the plate membrane stiffness; B_{ij} the membrane-bending coupling stiffness; and D_{ij} the bending stiffness; all for $i, j = 1, 2, 3$. The first Frechét derivative of the stress terms are:

$$\begin{aligned} N'_{ia} &= A_{ij}\varepsilon'_{ja} + B_{ij}\kappa'_{ja} \\ M'_{ia} &= B_{ij}\varepsilon'_{ja} + D_{ij}\kappa'_{ja} \end{aligned} \quad (33)$$

Recalling from Eq. 28 that $\kappa''_{jab} = 0$, the second Frechét derivatives are:

$$\begin{aligned} N''_{iab} &= A_{ij}\varepsilon''_{jab} \\ M''_{iab} &= B_{ij}\varepsilon''_{jab} \end{aligned} \quad (34)$$

Note that N''_{iab} , M''_{iab} are symmetric second-order tensors. The first derivatives with respect to λ can be readily computed as:

$$\begin{aligned} \dot{N}_i &= A_{ij}\dot{\varepsilon}_j + B_{ij}\dot{\kappa}_j \\ \dot{M}_i &= B_{ij}\dot{\varepsilon}_j + D_{ij}\dot{\kappa}_j \end{aligned} \quad (35)$$

$$\begin{aligned} \dot{N}'_{ia} &= A_{ij}\dot{\varepsilon}'_{ja} \\ \dot{M}'_{ia} &= B_{ij}\dot{\varepsilon}'_{ja} \end{aligned} \quad (36)$$

$$\begin{aligned} \dot{N}''_{iab} &= 0 \\ \dot{M}''_{iab} &= 0 \end{aligned} \quad (37)$$

Finally, the second derivatives about λ are:

$$\begin{aligned} \ddot{N}_i &= A_{ij}\ddot{\varepsilon}_j \\ \ddot{M}_i &= B_{ij}\ddot{\varepsilon}_j \\ \ddot{N}'_{ia} &= 0 \\ \ddot{M}'_{ia} &= 0 \\ \ddot{N}''_{iab} &= 0 \\ \ddot{M}''_{iab} &= 0 \end{aligned} \quad (38)$$

5.3. Functional Derivatives

Assuming a general loading vector with distributed forces $\hat{\mathbf{N}}$ at the plate boundaries $\delta\Omega$, the total potential energy can be written as:

$$\phi = \frac{1}{2} \int_{\Omega} (N_i \varepsilon_i + M_i \kappa_i) d\Omega - \int_{\delta\Omega} \lambda \hat{\mathbf{N}}^T \mathbf{u} d(\delta\Omega) \quad (39)$$

where $d\Omega = dx dy$ and summation convention is adopted for terms with repeated index i with $i = 1, 2, 3$. The stationary total potential energy at $[\mathbf{u}_c, \lambda_c]$ is defined as $\phi'_c = \phi'[\mathbf{u}_c, \lambda_c]$, calculated using the first variation of $\phi_c = \phi[\mathbf{u}_c, \lambda_c]$:

$$\begin{aligned} \phi'_c \delta\mathbf{u} &= \left[\frac{1}{2} \int_{\Omega} \left(\delta N_i \varepsilon_i + N_i \delta \varepsilon_i + \delta M_i \kappa_i + M_i \delta \kappa_i \right) d\Omega \right. \\ &\quad \left. - \int_{\delta\Omega} \lambda \hat{\mathbf{N}}^T \delta\mathbf{u} d(\delta\Omega) \right] \end{aligned} \quad (40)$$

The variation $\delta\mathbf{u}$ is defined as $\delta\mathbf{u} = \mathbf{u}_a = \{\dots, u_a, \dots\}^\top$, such that the first Frechét derivative of the total potential energy becomes:

$$\begin{aligned} \phi'_c \mathbf{u}_a &= \left[\frac{1}{2} \int_{\Omega} \left(N'_{ia} \varepsilon_i + N_i \varepsilon'_{ia} + M'_{ia} \kappa_i + M_i \kappa'_{ia} \right) d\Omega \right. \\ &\quad \left. - \int_{\delta\Omega} \lambda \hat{\mathbf{N}}^T S_{ax=\ell_x}^{\mathbf{u}} d(\delta\Omega) \right] u_a \end{aligned} \quad (41)$$

Resuming with the second Frechét derivative, now replacing $\delta\mathbf{u}$ with $\delta\mathbf{u} = \mathbf{u}_b = \{\dots, u_b, \dots\}^\top$:

$$\begin{aligned} \phi''_c \mathbf{u}_a \mathbf{u}_b &= \left[\frac{1}{2} \int_{\Omega} \left(N''_{iab} \varepsilon_i + N'_{ia} \varepsilon'_{ib} + N'_{ib} \varepsilon'_{ia} + N_i \varepsilon''_{iab} \right. \right. \\ &\quad \left. \left. + M''_{iab} \kappa_i + M'_{ia} \kappa'_{ib} + M'_{ib} \kappa'_{ia} + M_i \kappa''_{iab} \right)^0 d\Omega \right] u_a u_b \\ &= \left[\frac{1}{2} \int_{\Omega} \left(N''_{iab} \varepsilon_i + N'_{ia} \varepsilon'_{ib} + N'_{ib} \varepsilon'_{ia} + N_i \varepsilon''_{iab} \right. \right. \\ &\quad \left. \left. + M''_{iab} \kappa_i + M'_{ia} \kappa'_{ib} + M'_{ib} \kappa'_{ia} \right) d\Omega \right] u_a u_b \end{aligned} \quad (42)$$

Note that ϕ''_c in Eq. 42 represents a second-order tensor with all geometrically non-linear terms present. If a linear pre-buckling state is assumed, ϕ''_c becomes the linear constitutive stiffness matrix of the system [9]. Continuing with the third Frechét derivative, now using $\delta\mathbf{u} = \mathbf{u}_c = \{\dots, u_c, \dots\}^\top$:

$$\phi'''_c \mathbf{u}_a \mathbf{u}_b \mathbf{u}_c = \left[\frac{1}{2} \int_{\Omega} \left(\cancel{N''''_{iabc} \varepsilon_i}^0 + N''_{iab} \varepsilon'_{ic} + N''_{iac} \varepsilon'_{ib} \right) d\Omega \right]$$

$$\begin{aligned}
 & + N'_{ia}\overset{0}{\epsilon''}_{ibc} + N''_{ibc}\overset{0}{\epsilon'}_{ia} + N'_{ib}\overset{0}{\epsilon''}_{iac} + N'_{ic}\overset{0}{\epsilon''}_{iab} \\
 & + N_i\overset{0}{\epsilon'''_{abc}} + M''_{iabc}\overset{0}{\kappa'_i} + M''_{iab}\overset{0}{\kappa'_{ic}} + M''_{iac}\overset{0}{\kappa'_{ib}} \\
 & + M'_{ia}\overset{0}{\kappa''_{ibc}} + M''_{ibc}\overset{0}{\kappa'_{ia}} + M'_{ib}\overset{0}{\kappa''_{iac}} d\Omega \Big] u_a u_b u_c \\
 = & \left[\frac{1}{2} \int_{\Omega} \left(N''_{iab}\overset{0}{\epsilon'_{ic}} + N''_{iac}\overset{0}{\epsilon'_{ib}} + N'_{ia}\overset{0}{\epsilon''_{ibc}} \right. \right. \\
 & + N''_{ibc}\overset{0}{\epsilon'_{ia}} + N'_{ib}\overset{0}{\epsilon''_{iac}} + N'_{ic}\overset{0}{\epsilon''_{iab}} \\
 & \left. \left. + M''_{iab}\overset{0}{\kappa'_{ic}} + M''_{iac}\overset{0}{\kappa'_{ib}} + M''_{ibc}\overset{0}{\kappa'_{ia}} \right) d\Omega \right] u_a u_b u_c \quad (43)
 \end{aligned}$$

Lastly, using $\delta\mathbf{u} = \mathbf{u}_d = \{\dots, u_d, \dots\}^T$, the fourth Frechét derivative gives:

$$\begin{aligned}
 \phi_c^{iv} \mathbf{u}_a \mathbf{u}_b \mathbf{u}_c \mathbf{u}_d = & \left[\frac{1}{2} \int_{\Omega} \left(N''_{iabd}\overset{0}{\epsilon'_{ic}} + N''_{iab}\overset{0}{\epsilon''_{icd}} + N''_{iacd}\overset{0}{\epsilon''_{ib}} \right. \right. \\
 & + N''_{iac}\overset{0}{\epsilon''_{ibd}} + N''_{iad}\overset{0}{\epsilon''_{ibc}} + N'_{ia}\overset{0}{\epsilon'''_{ibcd}} + N''_{ibcd}\overset{0}{\epsilon'_{ia}} \\
 & + N''_{ibc}\overset{0}{\epsilon''_{iad}} + N''_{ibd}\overset{0}{\epsilon''_{iac}} + N'_{ib}\overset{0}{\epsilon'''_{iacd}} + N''_{icd}\overset{0}{\epsilon''_{iab}} \\
 & + N'_{ic}\overset{0}{\epsilon'''_{abd}} + M''_{iabd}\overset{0}{\kappa'_{ic}} + M''_{iab}\overset{0}{\kappa''_{icd}} + M''_{iacd}\overset{0}{\kappa'_{ib}} \\
 & \left. \left. + M''_{iac}\overset{0}{\kappa''_{ibd}} + M''_{ibd}\overset{0}{\kappa'_{ia}} + M''_{ibc}\overset{0}{\kappa''_{iad}} \right) d\Omega \right] u_a u_b u_c u_d \\
 = & \left[\frac{1}{2} \int_{\Omega} \left(N''_{iab}\overset{0}{\epsilon''_{icd}} + N''_{iac}\overset{0}{\epsilon''_{ibd}} + N''_{iad}\overset{0}{\epsilon''_{ibc}} \right. \right. \\
 & + N''_{ibc}\overset{0}{\epsilon''_{iad}} + N''_{ibd}\overset{0}{\epsilon''_{iac}} + N''_{icd}\overset{0}{\epsilon''_{iab}} \left. \left. \right) d\Omega \right] u_a u_b u_c u_d \quad (44)
 \end{aligned}$$

It is now possible to compute the functional differentiations corresponding to the second expansion of the total potential energy functional, about λ . From Eq. 42, the first differentiation about λ becomes:

$$\begin{aligned}
 \dot{\phi}_c'' \mathbf{u}_a \mathbf{u}_b = & \left[\frac{1}{2} \int_{\Omega} \left(\dot{N}'_{iab}\overset{0}{\epsilon'_i} + N''_{iab}\overset{0}{\dot{\epsilon}_i} + N'_{ia}\overset{0}{\dot{\epsilon}'_{ib}} \right. \right. \\
 & + N'_{ia}\overset{0}{\dot{\epsilon}'_{ib}} + \dot{N}'_{ib}\overset{0}{\epsilon'_{ia}} + N'_{ib}\overset{0}{\dot{\epsilon}'_{ia}} + \dot{N}_i\overset{0}{\epsilon''_{iab}} \\
 & + N_i\overset{0}{\dot{\epsilon}'''_{tab}} + M''_{iab}\overset{0}{\dot{\kappa}'_i} + M''_{iab}\overset{0}{\dot{\kappa}'_i} + \dot{M}'_{ia}\overset{0}{\kappa'_{ib}} \\
 & \left. \left. + M'_{ia}\overset{0}{\dot{\kappa}'_{ib}} + \dot{M}'_{ib}\overset{0}{\kappa'_{ia}} + M'_{ib}\overset{0}{\dot{\kappa}'_{ia}} \right) d\Omega \right] u_a u_b \\
 = & \left[\frac{1}{2} \int_{\Omega} \left(N''_{iab}\overset{0}{\dot{\epsilon}'_i} + N'_{ia}\overset{0}{\dot{\epsilon}'_{ib}} + N'_{ia}\overset{0}{\dot{\epsilon}'_{ib}} \right. \right. \\
 & + \dot{N}'_{ib}\overset{0}{\epsilon'_{ia}} + N'_{ib}\overset{0}{\dot{\epsilon}'_{ia}} + \dot{N}_i\overset{0}{\epsilon''_{iab}} + M''_{iab}\overset{0}{\dot{\kappa}'_i} \\
 & \left. \left. + \dot{M}'_{ia}\overset{0}{\kappa'_{ib}} + \dot{M}'_{ib}\overset{0}{\kappa'_{ia}} \right) d\Omega \right] u_a u_b \quad (45)
 \end{aligned}$$

The second differentiation of ϕ_c'' about λ becomes:

$$\begin{aligned}
 \ddot{\phi}_c'' \mathbf{u}_a \mathbf{u}_b = & \left[\frac{1}{2} \int_{\Omega} \left(\dot{N}'_{iab}\overset{0}{\dot{\epsilon}'_i} + N''_{iab}\overset{0}{\ddot{\epsilon}_i} + \dot{N}'_{ia}\overset{0}{\dot{\epsilon}'_{ib}} \right. \right. \\
 & + 2\dot{N}'_{ia}\overset{0}{\dot{\epsilon}'_{ib}} + N'_{ia}\overset{0}{\ddot{\epsilon}'_{ib}} + \dot{N}'_{ib}\overset{0}{\dot{\epsilon}'_{ia}} + 2\dot{N}'_{ib}\overset{0}{\dot{\epsilon}'_{ia}} \\
 & + N'_{ib}\overset{0}{\ddot{\epsilon}'_{ia}} + \dot{N}_i\overset{0}{\epsilon''_{iab}} + \dot{N}_i\overset{0}{\dot{\epsilon}'''_{tab}} + \dot{M}'_{ia}\overset{0}{\dot{\kappa}'_i} \\
 & + M''_{iab}\overset{0}{\ddot{\kappa}'_i} + \dot{M}'_{ia}\overset{0}{\kappa'_{ib}} + \dot{M}'_{ia}\overset{0}{\dot{\kappa}'_{ib}} \\
 & \left. \left. + \dot{M}'_{ib}\overset{0}{\kappa'_{ia}} + \dot{M}'_{ib}\overset{0}{\dot{\kappa}'_{ia}} \right) d\Omega \right] u_a u_b \\
 = & \left[\frac{1}{2} \int_{\Omega} \left(N''_{iab}\overset{0}{\ddot{\epsilon}'_i} + 2\dot{N}'_{ia}\overset{0}{\dot{\epsilon}'_{ib}} \right. \right. \\
 & + 2\dot{N}'_{ib}\overset{0}{\dot{\epsilon}'_{ia}} + \dot{N}_i\overset{0}{\epsilon''_{iab}} \left. \left. \right) d\Omega \right] u_a u_b \quad (46)
 \end{aligned}$$

The first differentiation of ϕ_c''' can be calculated based on Eq. 43 as:

$$\begin{aligned}
 \dot{\phi}_c''' \mathbf{u}_a \mathbf{u}_b \mathbf{u}_c = & \left[\frac{1}{2} \int_{\Omega} \left(\dot{N}'_{iab}\overset{0}{\dot{\epsilon}'_i} + N''_{iab}\overset{0}{\ddot{\epsilon}'_i} + \dot{N}'_{ia}\overset{0}{\dot{\epsilon}'_{ib}} \right. \right. \\
 & + N''_{iac}\overset{0}{\dot{\epsilon}'_{ib}} + \dot{N}'_{ia}\overset{0}{\dot{\epsilon}''_{ibc}} + N'_{ia}\overset{0}{\ddot{\epsilon}'''_{ibc}} + \dot{N}'_{ibc}\overset{0}{\dot{\epsilon}'_{ia}} \\
 & + N''_{ibc}\overset{0}{\dot{\epsilon}'_{ia}} + \dot{N}'_{ib}\overset{0}{\dot{\epsilon}''_{iac}} + N'_{ib}\overset{0}{\ddot{\epsilon}'''_{iac}} + \dot{N}'_{iac}\overset{0}{\dot{\epsilon}'_{ib}} \\
 & + N'_{ic}\overset{0}{\dot{\epsilon}'''_{tab}} + \dot{M}'_{iab}\overset{0}{\dot{\kappa}'_i} + M''_{iab}\overset{0}{\ddot{\kappa}'_i} + \dot{M}'_{iac}\overset{0}{\dot{\kappa}'_i} \\
 & \left. \left. + M''_{iac}\overset{0}{\ddot{\kappa}'_i} + \dot{M}'_{ibc}\overset{0}{\dot{\kappa}'_{ia}} + M''_{ibc}\overset{0}{\ddot{\kappa}'_{ia}} \right) d\Omega \right] u_a u_b u_c \\
 = & \left[\frac{1}{2} \int_{\Omega} \left(N''_{iab}\overset{0}{\ddot{\epsilon}'_i} + N''_{iac}\overset{0}{\dot{\epsilon}'_{ib}} + \dot{N}'_{ia}\overset{0}{\dot{\epsilon}''_{ibc}} \right. \right. \\
 & + N''_{ibc}\overset{0}{\dot{\epsilon}'_{ia}} + \dot{N}'_{ib}\overset{0}{\dot{\epsilon}''_{iac}} + \dot{N}'_{ic}\overset{0}{\dot{\epsilon}'''_{iac}} \left. \left. \right) d\Omega \right] u_a u_b u_c \quad (47)
 \end{aligned}$$

The second differentiation of ϕ_c''' about λ can be calculated from Eq. 47:

$$\begin{aligned}
 \ddot{\phi}_c''' \mathbf{u}_a \mathbf{u}_b \mathbf{u}_c = & \left[\frac{1}{2} \int_{\Omega} \left(\dot{N}'_{iab}\overset{0}{\dot{\epsilon}'_i} + N''_{iab}\overset{0}{\ddot{\epsilon}'_i} + \dot{N}'_{ia}\overset{0}{\dot{\epsilon}'_{ib}} \right. \right. \\
 & + N''_{iac}\overset{0}{\dot{\epsilon}'_{ib}} + \dot{N}'_{ia}\overset{0}{\dot{\epsilon}''_{ibc}} + N'_{ia}\overset{0}{\ddot{\epsilon}'''_{ibc}} + \dot{N}'_{ibc}\overset{0}{\dot{\epsilon}'_{ia}} \\
 & + N''_{ibc}\overset{0}{\dot{\epsilon}'_{ia}} + \dot{N}'_{ib}\overset{0}{\dot{\epsilon}''_{iac}} + N'_{ib}\overset{0}{\ddot{\epsilon}'''_{iac}} + \dot{N}'_{iac}\overset{0}{\dot{\epsilon}'_{ib}} \\
 & \left. \left. + \dot{N}'_{ic}\overset{0}{\dot{\epsilon}'''_{tab}} + \dot{M}'_{iab}\overset{0}{\dot{\kappa}'_i} + M''_{iab}\overset{0}{\ddot{\kappa}'_i} + \dot{M}'_{iac}\overset{0}{\dot{\kappa}'_i} \right) d\Omega \right] u_a u_b u_c = 0 \quad (48)
 \end{aligned}$$

The first and second differentiation of ϕ_c^{iv} with respect to λ can be calculated based on Eq. 44:

$$\begin{aligned} \dot{\phi}_c^{iv} \mathbf{u}_a \mathbf{u}_b \mathbf{u}_c \mathbf{u}_d = & \left[\frac{1}{2} \int_{\Omega} \left(\dot{N}_{iab}^v \epsilon_{icd}'' + N_{iab}'' \dot{\epsilon}_{icd}'' + \dot{N}_{iac}^v \epsilon_{ibd}'' \right. \right. \\ & + N_{iac}'' \dot{\epsilon}_{ibd}'' + \dot{N}_{iad}^v \epsilon_{ibc}'' + N_{iad}'' \dot{\epsilon}_{ibc}'' + \dot{N}_{ibc}^v \epsilon_{iad}'' \\ & + N_{ibc}'' \dot{\epsilon}_{iad}'' + \dot{N}_{ibd}^v \epsilon_{iac}'' + N_{ibd}'' \dot{\epsilon}_{iac}'' \\ & \left. \left. + \dot{N}_{icd}^v \epsilon_{iab}'' + N_{icd}'' \dot{\epsilon}_{iab}'' \right) d\Omega \right] \mathbf{u}_a \mathbf{u}_b \mathbf{u}_c \mathbf{u}_d = 0 \quad (49) \end{aligned}$$

$$\ddot{\phi}_c^{iv} \mathbf{u}_a \mathbf{u}_b \mathbf{u}_c \mathbf{u}_d = 0 \quad (50)$$

6. Modified Bogner-Fox-Schmit Finite Element

The Bogner-Fox-Schmit (BFS) finite element [39] is a classical C1 contiguous confirming plate element obtained by taking tensor products of cubic Hermite splines. The BFS is one of the most accurate rectangular finite elements for thin-walled shells, as stated by Zienkiewicz & Taylor [40, p. 153], and therefore has been chosen to implement the formulation herein developed. With only 4 nodes per element, the standard BFS element approximates the out-of-plane displacements using 3rd-order polynomials, which is still a reasonable low-order interpolation for plates and very simple to implement [56], in contrast with triangular elements which use higher order polynomials [56], such as the Argyris element [57].

A drawback of the standard BFS element when used in the context of Koiter's method is the linear interpolation of the in-place displacements [39], resulting in a poor convergence when trying to represent the second-order displacement fields \mathbf{u}_{ij} and all dependent quantities such as the $b_{ijk\ell}$ factors of Eq. 19.

A modified BFS element is proposed to enable third-order interpolation also for the in-plane displacements. Additional 4 degrees-of-freedom per node are included, being the first derivatives of the in-plane displacements: $u_{,x}$, $u_{,y}$, $v_{,x}$ and $v_{,y}$. Hence, no nodes are added and the resulting element has still 4 nodes with 10 degrees-of-freedom per node. This enhanced BFS element is referred to in the following discussion as BFSC: Bogner-Fox-Schmit-Castro. The in-plane u , v and out-of-plane w displacements are approximated using:

$$u, v, w = \sum_{i=1}^4 \mathbf{S}_i^{u,v,w} \mathbf{u}_{ei} \quad (51)$$

where \mathbf{u}_{ei} contains the 10 degrees-of-freedom of the i^{th} node. The matrices containing the shape functions $\mathbf{S}_i^{u,v,w}$ are defined as:

$$\begin{aligned} \mathbf{S}_i^u &= \begin{bmatrix} H_i & H_i^x & H_i^y & 0 & 0 & 0 & 0 & 0 & 0 & 0 \end{bmatrix} \\ \mathbf{S}_i^v &= \begin{bmatrix} 0 & 0 & 0 & H_i & H_i^x & H_i^y & 0 & 0 & 0 & 0 \end{bmatrix} \\ \mathbf{S}_i^w &= \begin{bmatrix} 0 & 0 & 0 & 0 & 0 & 0 & H_i & H_i^x & H_i^y & H_i^{xy} \end{bmatrix} \end{aligned} \quad (52)$$

with $H_i, H_i^x, H_i^y, H_i^{xy}$ calculated using natural coordinates [58, 59, 60]:

$$\begin{aligned} H_i &= \frac{1}{16}(\xi + \xi_i)^2(\xi\xi_i - 2)(\eta + \eta_i)^2(\eta\eta_i - 2) \\ H_i^x &= -\frac{\ell_x}{32}\xi_i(\xi + \xi_i)^2(\xi\xi_i - 1)(\eta + \eta_i)^2(\eta\eta_i - 2) \\ H_i^y &= -\frac{\ell_y}{32}(\xi + \xi_i)^2(\xi\xi_i - 2)\eta_i(\eta + \eta_i)^2(\eta\eta_i - 1) \\ H_i^{xy} &= \frac{\ell_x\ell_y}{64}\xi_i(\xi + \xi_i)^2(\xi\xi_i - 1)\eta_i(\eta + \eta_i)^2(\eta\eta_i - 1) \end{aligned} \quad (53)$$

where ℓ_x, ℓ_y are respectively the finite element dimensions along x, y . The values of ξ_i, η_i given in Eq. 54 were adopted for each of the four nodes.

Node	ξ_i	η_i
1	-1	-1
2	+1	-1
3	+1	+1
4	-1	+1

(54)

In the present study, only rectangular elements were used, such that the natural coordinates can be defined simply as: $\xi = 2x/\ell_x - 1$; and $\eta = 2y/\ell_y - 1$. All derivatives of $\mathbf{S}_i^{u,v,w}$ required in the strain equations can then be calculated in terms of the natural coordinates using Eq. 55. All integrations over the finite element domains are performed numerically using standard Gauss-quadrature and a mesh of 4×4 integration points per element, unless otherwise specified.

$$\begin{aligned} \frac{\partial}{\partial x} &= \frac{\ell_x}{2} \frac{\partial}{\partial \xi} \\ \frac{\partial}{\partial y} &= \frac{\ell_y}{2} \frac{\partial}{\partial \eta} \end{aligned} \quad (55)$$

7. Implementation

The main challenge to implement Koiter's asymptotic approach is the calculation of the third- and fourth-order tensors ϕ_c''' and ϕ_c^{iv} . A naive implementation can easily blow the memory of any modern computer. For example, a mesh with only 20 nodes, or 200 degrees of freedom using the BFSC element, would generate a complete ϕ_c^{iv} tensor with $200^4 = 1.6 \times 10^9$ elements to be stored, requiring 11.92 GB of memory if double precision is used. Moreover, calculating all 1.6×10^9 terms is computationally too expensive. For slightly larger problems found in any engineering application such naive approach becomes just impracticable. Many drawbacks experienced in the past with Koiter's asymptotic method are due to mistakes in implementation more than to intrinsic defects of the asymptotic approach itself, as stated by Casciaro [9]. The implementation herein proposed carefully takes into account all non-zero terms derived in Section 5.3 while calculating the higher-order tensors. The strategy adopted consists on evaluating the products involving high-order tensors ϕ_c''' and ϕ_c^{iv} on-the-fly, already during the numerical integration of each element. For instance, ϕ_c^{iv} defined in Eq. 44 is never fully calculated. Instead, the tensor

product $\phi_c^{iv} \mathbf{u}_a \mathbf{u}_b \mathbf{u}_c \mathbf{u}_d$ is evaluated and stored during the finite element assembly, using the following rearrangement of Eq. 44:

$$\begin{aligned} \phi_c^{iv} \mathbf{u}_a \mathbf{u}_b \mathbf{u}_c \mathbf{u}_d = & \frac{1}{2} \sum_{e=1}^k \int_{\Omega^e} \left(u_a u_b N''_{iab} \epsilon''_{icd} u_c u_d \right. \\ & + u_a u_c N''_{iac} \epsilon''_{ibd} u_b u_d + u_a u_d N''_{iad} \epsilon''_{ibc} u_b u_c \\ & + u_b u_c N''_{ibc} \epsilon''_{iad} u_a u_d + u_b u_d N''_{ibd} \epsilon''_{iac} u_a u_c \\ & \left. + u_c u_d N''_{icd} \epsilon''_{iab} u_a u_b \right) d\Omega^e \end{aligned} \quad (56)$$

where Ω^e represents the domain of one finite element. Note that only tensors up to second-order are fully calculated and stored, e.g. N_{iab}, ϵ_{ibd} . Moreover, for the implementation one should note that $N_{iab} = N_{iac} = N_{iad} = N_{ibc} = N_{ibd} = N_{icd}$ and $\epsilon_{iab} = \epsilon_{iac} = \epsilon_{iad} = \epsilon_{ibc} = \epsilon_{ibd} = \epsilon_{icd}$, such that ϵ_{iab} is calculated with Eq. 28 and N_{iab} with Eq. 34. The implementation carried out for the present study is based on Python [61], NumPy [62] and Cython [63], where all tensor products are efficiently evaluated using NumPy [62], as illustrated in the following pseudo-code:

```
from numpy import einsum
...
phi4 = 0
for point in integration_points:
    weight = compute_weight(point)
    Niab = compute_Niab(point)
    eicd = compute_eicd(point)
    phi4 += 1/2 * weight * einsum('iab,icd,a,b,c,d',
                                   Niab, eicd, ua, ub, uc, ud)
```

The authors could verify the benefit of the proposed formulation and notation while implementing the method, achieving a one-to-one correspondence between the method and implemented algorithms.

8. Results for single-mode Koiter's asymptotic expansion

8.1. Isotropic plates

Lanzo et al. [64] performed initial post-buckling analysis in isotropic plates with various aspect ratios, loading and boundary conditions, as illustrated in Figure 1. Table 1 compares the convergence of $\lambda_c / \lambda_{ref}$ with

$$\lambda_{ref} = \frac{\pi^2}{b^2} \frac{Eh^3}{12(1-\nu^2)}$$

Table 2 shows the convergence of b_I , often referred to in the literature dealing single-mode asymptotic expansion as the "b-factor". The results from Lanzo et al. [64] are compared against the BFSC implementation with progressively refined meshes. The mesh refinement is controlled by the number of elements along y , named n_y , calculating the number of elements along x using $n_x = a/b \times n_y$. The numerical integration was done using 4x4 integration points, which

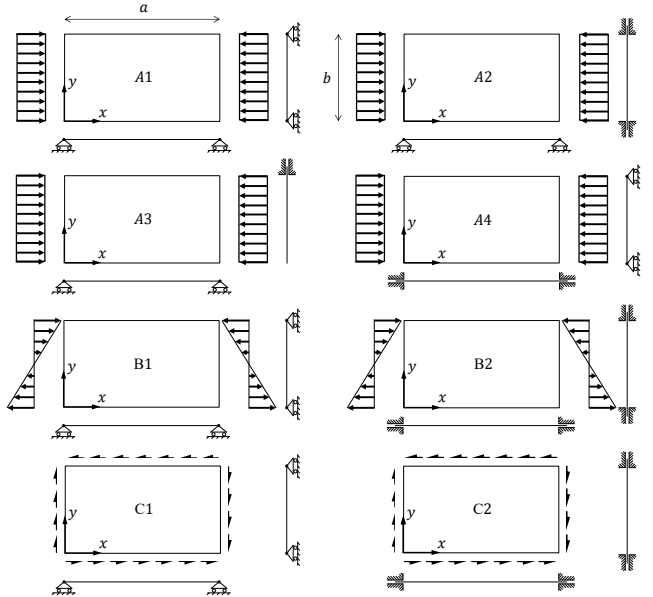


Figure 1: Models for isotropic plates, adapted from Lanzo et al. [64]

provided a converged and stable integration scheme, i.e. we verified that adding more integration points did not change the results and using less integration points (3x3) resulted in unstable behaviour for models B1, B2, C1 and C2.

The first buckling mode \mathbf{u}_1 and corresponding second-order field \mathbf{u}_{11} for each all models with $a/b = 3$ are given in Figures 3 - 4. Those results correspond to a mesh of $(n_x = 60) \times (n_y = 20)$ BFSC elements. The plots are created using a visualization mesh of 900×300 points along x and y , respectively; calculating the consistent displacement according to Eq. 52 at each plotting point. Note the complexity of the second-order displacement, which are in-plane for this case. The fast convergence for b_I shown in Table 2 is a direct consequence of the fast convergence of the second-order field \mathbf{u}_{11} . The enrichment on u and v enabled by the BFSC element is the main reason for this fast-converging behavior.

8.2. Composite plates

A composite plate presented by Phan & Reddy [65] and Bilotta et al. [66] will be used as a reference for verification of the single-mode expansion for composite plates. The following material properties are used:

$$E_2 = 8 \text{ GPa}, \quad \frac{G_{12}}{E_2} = 0.6, \quad \nu_{12} = 0.25$$

Using the load and boundary conditions of model A1 of Fig. 1, the plate geometry is defined based on $a = b = 1 \text{ m}$, and thickness of $h = 0.1 \text{ m}$. The laminate stacking sequence is $[0/90/90/0]$, with the principal direction being the plate's x -axis. Table 3 shows the convergence of the critical linear buckling eigenvalue for the BFSC element. The results from Phan & Reddy [65] are exact solutions obtained with classical plate theory, whereas the results from [66] are based on

Table 1
Convergence of BFSC element for first buckling mode, isotropic case

Model	Case	Lanzo et al. [64]		BFSC convergence for λ_c/λ_{ref}								
		$n_x \times n_y$	λ_c/λ_{ref}	$n_y = 4$	$n_y = 6$	$n_y = 8$	$n_y = 10$	$n_y = 12$	$n_y = 14$	$n_y = 16$	$n_y = 18$	$n_y = 20$
A1	$a/b = 1$	25×25	4.00263	3.99358	3.99921	3.99983	3.99995	3.99998	3.99999	4.00000	4.00000	4.00000
	$a/b = 2$	49×21	4.00323	3.99419	3.99929	3.99985	3.99996	3.99998	3.99999	4.00000	4.00000	4.00000
	$a/b = 3$	49×15	4.00674	3.99439	3.99932	3.99985	3.99996	3.99998	3.99999	4.00000	4.00000	4.00000
A2	$a/b = 1$	33×33	7.71346	7.66910	7.69296	7.69263	7.69203	7.69171	7.69154	7.69145	7.69139	7.69136
	$a/b = 2$	49×21	7.01142	6.95834	6.97190	6.97210	6.97191	6.97178	6.97171	6.97167	6.97165	6.97163
	$a/b = 3$	-	-	7.03814	7.05577	7.05595	7.05565	7.05547	7.05531	7.05528	7.05526	-
A3	$a/b = 1$	-	-	1.69586	1.69768	1.69806	1.69817	1.69821	1.69823	1.69824	1.69825	1.69825
	$a/b = 2$	33×17	1.38808	1.38371	1.38566	1.38602	1.38612	1.38616	1.38618	1.38619	1.38619	1.38619
	$a/b = 3$	-	-	1.33821	1.33894	1.33908	1.33912	1.33914	1.33914	1.33915	1.33915	1.33915
A4	$a/b = 1$	-	-	6.73286	6.74461	6.74418	6.74373	6.74350	6.74337	6.74331	6.74327	6.74324
	$a/b = 2$	49×21	4.85495	4.83580	4.84603	4.84698	4.84713	4.84715	4.84716	4.84716	4.84716	4.84715
	$a/b = 3$	-	-	4.39779	4.40549	4.40627	4.40642	4.40645	4.40646	4.40646	4.40646	4.40646
B1	$a/b = 1$	33×33	25.57659	24.19007	25.40526	25.50502	25.52282	25.52721	25.52846	25.52882	25.52889	25.52887
	$a/b = 2$	49×23	23.94518	23.30597	23.83356	23.87513	23.88171	23.88292	23.88303	23.88291	23.88275	23.88261
	$a/b = 3$	49×15	24.2542	23.51109	24.07096	24.10957	24.11329	24.11343	24.11343	24.11292	24.11273	-
B2	$a/b = 1$	33×33	48.15739	50.37432	48.28268	47.93517	47.83308	47.79429	47.77688	47.76807	47.76321	47.76033
	$a/b = 2$	49×23	42.21176	42.88262	41.91507	41.73877	41.68699	41.66723	41.65827	41.65367	41.65109	41.64952
	$a/b = 3$	49×15	41.72252	41.53774	40.70907	40.55857	40.51447	40.49763	40.48996	40.48601	40.48377	40.48241
C1	$a/b = 1$	25×25	9.35185	8.71909	9.24793	9.31349	9.32538	9.32769	9.32784	9.32749	9.32708	9.32670
	$a/b = 2$	45×23	6.56822	6.54374	6.55314	6.55058	6.54903	6.54813	6.54757	6.54720	6.54695	6.54678
	$a/b = 3$	45×15	5.88460	5.95400	5.89677	5.87237	5.86074	5.85441	5.85060	5.84813	5.84645	5.84525
C2	$a/b = 1$	25×25	14.78220	14.92525	14.74298	14.68146	14.66129	14.65341	14.64965	14.64755	14.64623	14.64535
	$a/b = 2$	45×23	10.34334	10.74294	10.44685	10.35511	10.31516	10.29405	10.28156	10.27355	10.26811	10.26424
	$a/b = 3$	45×15	9.74613	9.67930	9.56774	9.54651	9.54032	9.53787	9.53667	9.53599	9.53557	9.53530

Table 2
Convergence of BFSC element for b_I (b -factor), isotropic case

Model	Case	Lanzo et al. [64]		BFSC convergence for b_I (b -factor)								
		$n_x \times n_y$	$b_{I=1}$	$n_y = 4$	$n_y = 6$	$n_y = 8$	$n_y = 10$	$n_y = 12$	$n_y = 14$	$n_y = 16$	$n_y = 18$	$n_y = 20$
A1	$a/b = 1$	25×25	0.18244	0.18655	0.18373	0.18311	0.18289	0.18279	0.18273	0.18270	0.18267	0.18266
	$a/b = 2$	49×21	0.21177	0.21517	0.21277	0.21222	0.21202	0.21193	0.21188	0.21185	0.21183	0.21182
	$a/b = 3$	49×15	0.22167	0.22519	0.22302	0.22251	0.22232	0.22224	0.22219	0.22216	0.22214	0.22212
A2	$a/b = 1$	33×33	0.19576	0.21278	0.26446	0.19664	0.21681	0.19589	0.20598	0.19571	0.20176	0.19565
	$a/b = 2$	49×21	0.26541	0.27179	0.26607	0.26500	0.26467	0.26452	0.26447	0.26443	0.26441	0.26440
	$a/b = 3$	-	-	0.33573	0.33077	0.32955	0.32911	0.32904	0.32897	0.32893	0.32891	0.32889
A3	$a/b = 1$	-	-	0.00619	0.00529	0.00504	0.00493	0.00488	0.00485	0.00482	0.00481	0.00480
	$a/b = 2$	33×17	0.00881	0.00951	0.00912	0.00900	0.00895	0.00892	0.00891	0.00890	0.00889	0.00889
	$a/b = 3$	-	-	0.02572	0.02600	0.02507	0.02528	0.02497	0.02509	0.02494	0.02501	0.02492
A4	$a/b = 1$	-	-	0.17106	0.17037	0.17023	0.17015	0.17011	0.17009	0.17007	0.17006	0.17005
	$a/b = 2$	49×21	0.26083	0.31749	0.27225	0.26075	0.26085	0.26367	0.26339	0.26047	0.25998	0.26069
	$a/b = 3$	-	-	0.18543	0.18392	0.18358	0.18346	0.18341	0.18337	0.18336	0.18334	0.18333
B1	$a/b = 1$	33×33	0.21935	0.21531	0.33212	0.22298	0.24930	0.22145	0.23232	0.22108	0.22622	0.22094
	$a/b = 2$	49×23	0.21960	0.24769	0.23083	0.23598	0.22395	0.23024	0.22380	0.22462	0.22473	0.22321
	$a/b = 3$	49×15	0.21148	0.21735	0.26961	0.22659	0.21428	0.22178	0.21473	0.21194	0.21577	0.21416
B2	$a/b = 1$	33×33	0.29241	0.39369	0.34365	0.39354	0.30060	0.31165	0.30953	0.30172	0.29923	0.29945
	$a/b = 2$	49×23	0.28583	0.34901	0.33925	0.32215	0.28414	0.29305	0.28055	0.28671	0.28312	0.28326
	$a/b = 3$	49×15	0.27654	0.33651	0.34539	0.31122	0.28495	0.28404	0.27896	0.27751	0.27998	0.27734
C1	$a/b = 1$	25×25	0.11453	0.10765	0.11914	0.11926	0.11897	0.11877	0.11864	0.11855	0.11849	0.11845
	$a/b = 2$	45×23	0.07171	0.07680	0.07527	0.07465	0.07448	0.07424	0.07417	0.07412	0.07409	0.07407
	$a/b = 3$	45×15	0.07992	0.11259	0.09853	0.09254	0.08860	0.08632	0.08505	0.08429	0.08383	0.08353
C2	$a/b = 1$	25×25	0.11686	0.15020	0.12852	0.12391	0.12229	0.12159	0.12124	0.12104	0.12092	0.12084
	$a/b = 2$	45×23	0.13282	0.11883	0.17133	0.15872	0.15760	0.14789	0.14515	0.14331	0.14308	0.14044
	$a/b = 3$	45×15	0.08651	0.10179	0.09192	0.08984	0.08913	0.08883	0.08868	0.08860	0.08855	0.08851

bi-quadratic finite elements and a mesh of 25×25 elements. Note the good agreement between the BFSC element and the literature for all anisotropic ratios E_1/E_2 , already with a mesh of only 4×4 elements.

The convergence of the b_I coefficient is shown in Table 4. The second-order displacement field \mathbf{u}_{11} was solved with Eq.

13 and orthogonalized with Eq. 14. Note in Figure 6 how the $u, v, \sqrt{u^2 + v^2}$ displacement components of \mathbf{u}_{11} change with the anisotropic ratio E_1/E_2 , clearly showing that in the initial post-buckling the displacements are progressively more focused with the increase of E_1/E_2 , and that these focused post-buckling displacements are aligned with the 0° and 90°

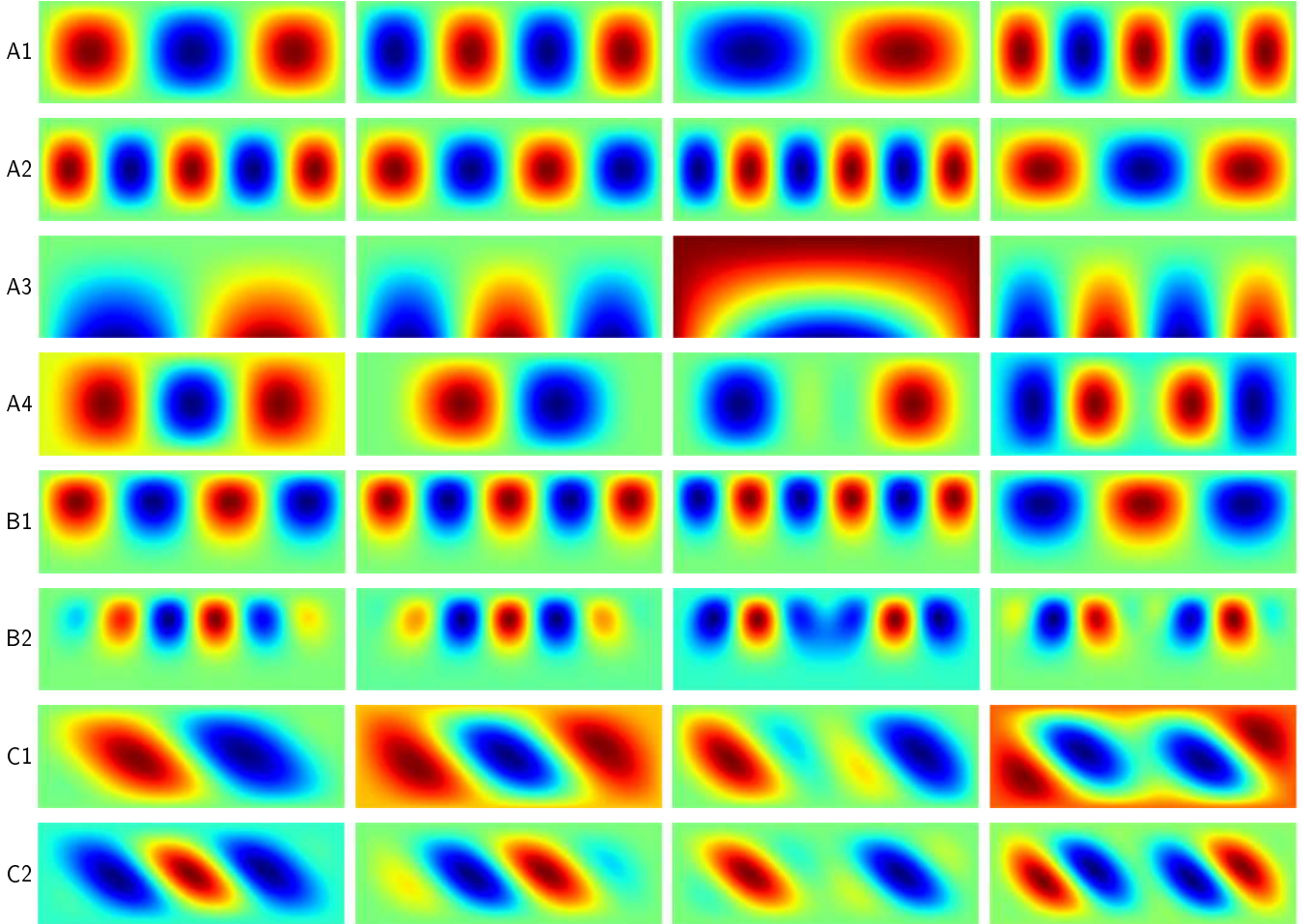


Figure 2: \mathbf{u}_I for isotropic plates with $a/b = 3$; each row corresponds to one model; columns from left to right are linear buckling modes for: $I = 1, 2, 3, 4$

Table 3

Convergence of BFSC element for first buckling mode and model A1 with $a/b = 1$, anisotropic case

E_1/E_2	Phan & Reddy [65] λ_c/λ_{ref}	BFSC convergence for λ_c/λ_{ref}								
		$n_y = 4$	$n_y = 6$	$n_y = 8$	$n_y = 10$	$n_y = 12$	$n_y = 14$	$n_y = 16$	$n_y = 18$	$n_y = 20$
1	-	4.1596	4.1662	4.1670	4.1671	4.1671	4.1672	4.1671	4.1671	4.1671
3	5.7538	5.7561	5.7501	5.7534	5.7537	5.7538	5.7537	5.7538	5.7540	5.7540
10	11.492	11.4976	11.4923	11.4922	11.4919	11.4919	11.4921	11.4919	11.4914	11.4916
20	19.712	19.7148	19.7167	19.7135	19.7127	19.7127	19.7119	19.7124	19.7122	19.7144

directions of the laminate stacking sequence.

9. Results for multi-mode Koiter's asymptotic expansion

9.1. Isotropic plates

Tiso [10] presented multi-modal results for model A1 using a geometry of: $a = 0.14\text{ m}$, $b = 0.10\text{ m}$ and thickness of 1 mm ; with isotropic material properties $E = 70\text{ GPa}$ and $\nu = 0.3$. With this configuration, the first two buckling loads are close and respectively equal to 2828.15 N and 2866.50 N . Tiso's definition of coefficients $b_{ijk\ell}$ can be translated to the notation herein presented as given in Eq. 57, which has a different index ordering when compared to

Eq. 19. Despite the different index ordering, Eq. 19 and Eq. 57 are equivalent in cases where $a_{ijk} = 0$.

$$b_{ijk\ell}^{\text{Tiso}} = -\frac{\frac{1}{6}\phi_c^{iv}\mathbf{u}_i\mathbf{u}_j\mathbf{u}_k\mathbf{u}_\ell + \frac{1}{2}\phi_c'''\mathbf{u}_k\mathbf{u}_\ell\mathbf{u}_{ij} + \frac{1}{2}\phi_c'''\mathbf{u}_\ell\mathbf{u}_i\mathbf{u}_{jk}}{\lambda_i\dot{\phi}_c''\mathbf{u}_\ell\mathbf{u}_\ell} \quad (57)$$

Table 5 show the verification of the formulation herein presented against the results from Tiso [10] for a multi-modal expansion using 2 modes.

Jansen & Rahman [67] used the general purpose finite element code DIANA [68] to investigate the dynamic response of plates and shells using reduced-order models based on

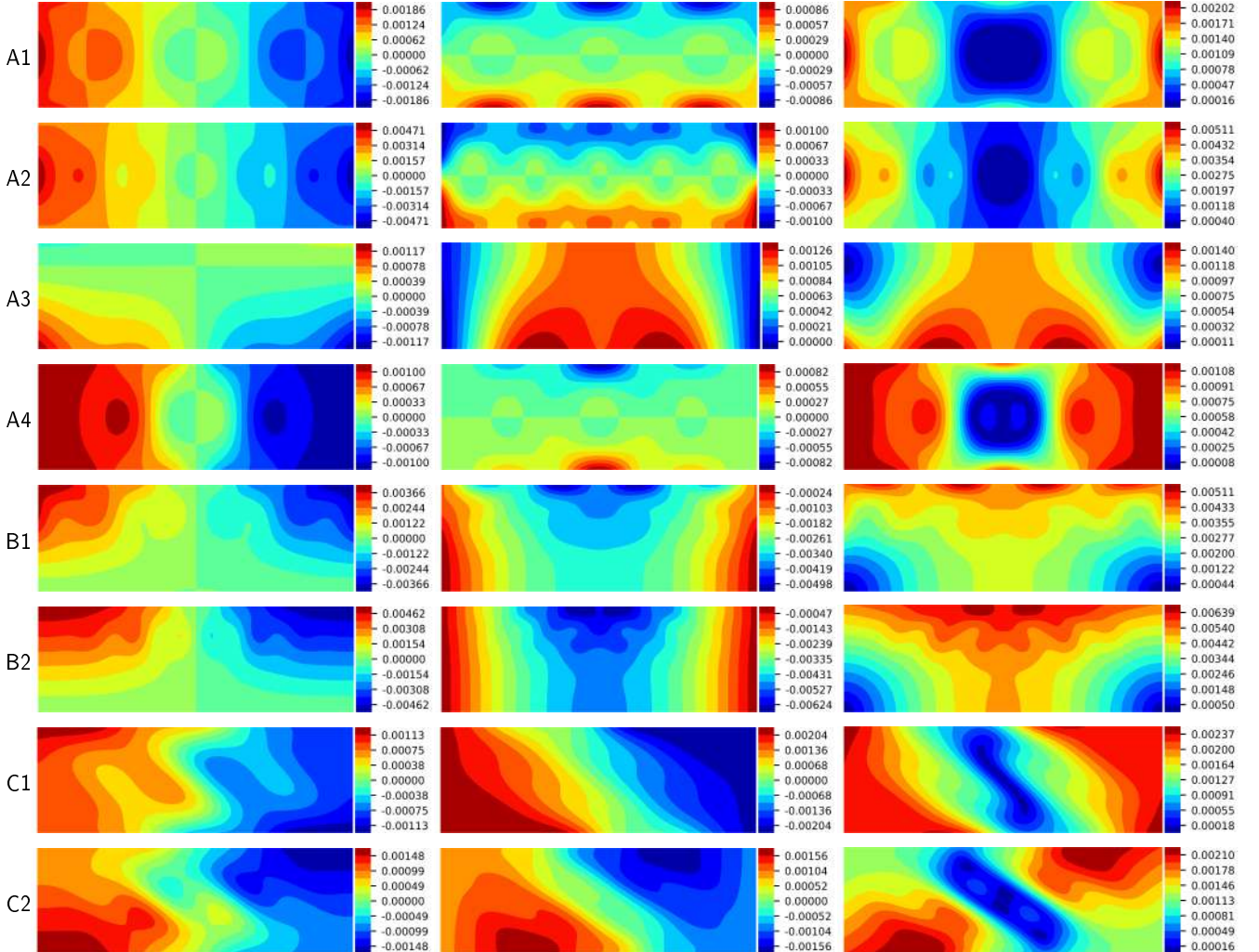


Figure 3: u_{11} for isotropic plate with $a/b = 3$; each row corresponds to one model; columns from left to right are: u , v , $\sqrt{u^2 + v^2}$

Table 4

Convergence of BFSC element for b_I (b -factor), model A1 with $a/b = 1$, anisotropic case

E_1/E_2	Bilotta et al. [66]	BFSC convergence for b_I (b -factor)								
		$n_y = 4$	$n_y = 6$	$n_y = 8$	$n_y = 10$	$n_y = 12$	$n_y = 14$	$n_y = 16$	$n_y = 18$	$n_y = 20$
1	-	0.17403	0.17138	0.17078	0.17056	0.17046	0.17041	0.17038	0.17036	0.17034
3	0.19865	0.20384	0.20011	0.19933	0.19906	0.19894	0.19887	0.19883	0.19880	0.19878
10	0.17075	0.17792	0.17277	0.17172	0.17135	0.17117	0.17108	0.17103	0.17100	0.17098
20	0.12595	0.13393	0.12809	0.12689	0.12646	0.12627	0.12616	0.12609	0.12604	0.12607

Koiter's theory. The plate therein investigated has a geometry of $a = 0.6 \text{ m}$, $b = 0.2 \text{ m}$, total thickness of 1 mm . The same plate was used to verify the formulation and implementation herein presented for the multi-modal asymptotic expansion of a composite plate. Using the loading and boundary condition of model A1 (Figure 1, the analyses in DIANA are carried out using two element types: **1**) The eight-node quadrilateral shell element CQ40L, based on first-order shear deformation kinematics (FSDT), mesh with 16×48 elements; **2**) Allman-type triangular element [69, 70], with kinematics based on the classical laminated plate the-

ory (CLPT). The Allman-type element triangular mesh has $24 \times 72 \times 2$ elements. Table 6 presents the linear buckling eigenvalues and Table 7 presents the results for the $b_{ijk\ell}$ coefficients using 5 modes, calculated per Eq. 19 for a plate with isotropic properties $E = 70 \text{ GPa}$ and $\nu = 0.3$. The relative error is calculated about the results using DIANA's Allman-type element. The BFSC mesh has 16×48 elements, and the authors verified that all models are converged. There is clearly a close agreement between DIANA's implementation and the present formulation, with a maximum difference of 9%, attributed to differences verified for the linear buck-

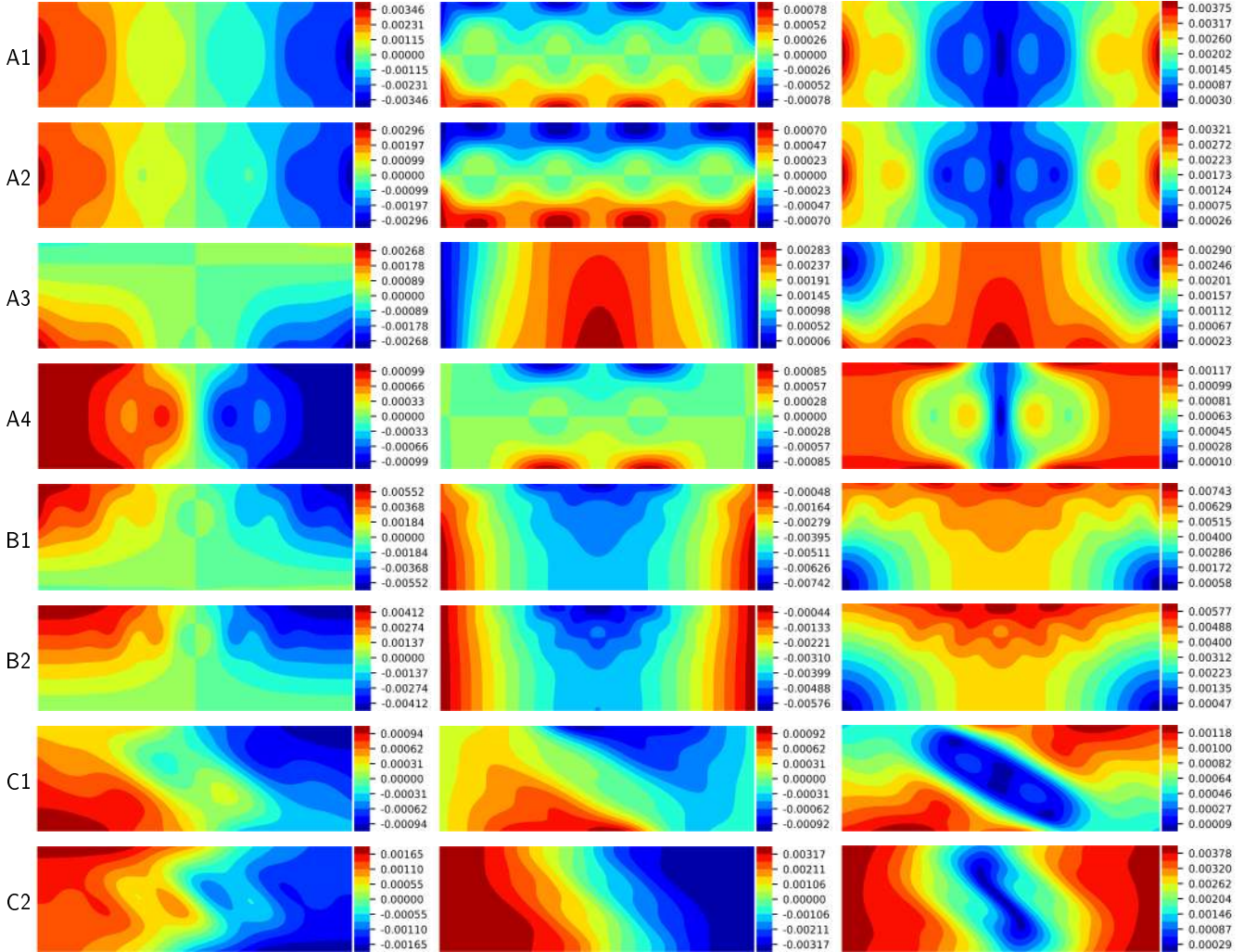


Figure 4: \mathbf{u}_{22} for isotropic plate with $a/b = 3$; each row corresponds to one model; columns from left to right are: u , v , $\sqrt{u^2 + v^2}$

Table 5

Multi-modal expansion coefficients $b_{ijk\ell}^{Tiso}$ for isotropic plate

$b_{1jk\ell}^{Tiso}$	Tiso [10]	BFSC	$b_{2jk\ell}^{Tiso}$	Tiso [10]	BFSC
b_{1111}	0.1353	0.1347	b_{2111}	0	0
b_{1112}	0	0	b_{2112}	0.0663	0.0682
b_{1121}	0	0	b_{2121}	0.2796	0.2543
b_{1122}	0.0663	0.0692	b_{2122}	0	0
b_{1211}	0	0	b_{2211}	0.2747	0.2729
b_{1212}	0.0675	0.0644	b_{2212}	0	0
b_{1221}	0.2747	0.2766	b_{2221}	0	0
b_{1222}	0	0	b_{2222}	0.2221	0.2176

Table 6

Eigenvalues λ_i for isotropic plate used in multi-modal analysis, units in $[N/m]$

Eigenvalue	DIANA CQ40L	DIANA Allman	BFSC
λ_1	6307	6337	6328
λ_2	6844	6885	6866
λ_3	7405	7432	7426
λ_4	8105	8165	8127
λ_5	9863	9955	9886
λ_6	12040	12182	12066
λ_7	14606	14822	14635
λ_8	17542	17584	17575

ling eigenvalues λ_i , shown in Table 6. For many coefficients, there is a sign switch because \mathbf{u}_i are symmetric eigenmodes about the plate mid-plane, providing interchangeably positive and negative solution for some of the $b_{ijk\ell}$ coefficients.

Figure 7 illustrates the second-order field modes \mathbf{u}_{ij} for the isotropic plate used in the multi-modal asymptotic ex-

pansion.

9.2. Composite plates

Table 8 presents the linear buckling eigenvalues and Table 9 present results for a composite plate with layup of $[+45/-45/90/0]_{sym}$ and material properties $E_{11} =$

Table 7Multi-modal expansion coefficients $b_{ijk\ell}$ for isotropic plate using 5 modes

$b_{ijk\ell}$	DIANA CQ40L	DIANA Allman	BFSC	Err	$b_{ijk\ell}$	DIANA CQ40L	DIANA Allman	BFSC	Err	$b_{ijk\ell}$	DIANA CQ40L	DIANA Allman	BFSC	Err	$b_{ijk\ell}$	DIANA CQ40L	DIANA Allman	BFSC	Err	$b_{ijk\ell}$	DIANA CQ40L	DIANA Allman	BFSC	Err	
b_{1111}	0.21531	0.21756	0.21564	1%	b_{1111}	0	0	0	0	b_{1111}	0	0	0	0	b_{1111}	0.01072	0.01079	0.01084	0%	b_{1111}	0	0	0	0	
b_{1112}	0	0	0	0	b_{1112}	0.11844	0.11830	0.11971	1%	b_{1112}	-0.11414	0.11583	0.10853	6%	b_{1112}	0	0	0	0	b_{1112}	-0.01003	0.01004	-0.01012	1%	
b_{1113}	0	0	0	0	b_{1113}	0.03165	0.03132	0.02935	6%	b_{1113}	0.15488	0.16034	0.16034	2%	b_{1113}	0	0	0	0	b_{1113}	0.03535	0.0349	-0.0352	1%	
b_{1114}	0.03791	0.03852	0.03868	0%	b_{1114}	0	0	0	0	b_{1114}	0.01732	0.16034	0.16034	0	b_{1114}	0.09640	0.09693	0.09810	1%	b_{1114}	0	0	0	0	
b_{1115}	0	0	0	0	b_{1115}	-0.03296	0.03256	-0.03278	1%	b_{1115}	0.04183	0.04190	-0.04218	1%	b_{1115}	0	0	0	0	b_{1115}	0.07800	0.07834	0.07940	1%	
b_{1121}	0	0	0	0	b_{1121}	0.10201	0.10181	0.09619	6%	b_{1121}	-0.13375	0.13454	0.14553	8%	b_{1121}	0	0	0	0	b_{1121}	-0.1008	0.01006	-0.01014	1%	
b_{1122}	0.22357	0.22823	0.23092	1%	b_{1122}	0	0	0	0	b_{1122}	0	0	0	0	b_{1122}	-0.02560	-0.02558	-0.02360	8%	b_{1122}	0	0	0	0	
b_{1123}	-0.05975	0.06042	0.05661	6%	b_{1123}	0	0	0	0	b_{1123}	0	0	0	0	b_{1123}	0.02485	-0.02539	-0.02385	6%	b_{1123}	0	0	0	0	
b_{1124}	0	0	0	0	b_{1124}	-0.00139	-0.00116	-0.00643	6%	b_{1124}	0.14851	-0.15510	-0.14599	6%	b_{1124}	0	0	0	0	b_{1124}	-0.1931	0.01934	-0.1798	7%	
b_{1125}	-0.06222	0.06282	-0.06322	1%	b_{1125}	0	0	0	0	b_{1125}	0	0	0	0	b_{1125}	-0.07448	0.07506	-0.07873	5%	b_{1125}	0	0	0	0	
b_{1131}	0	0	0	0	b_{1131}	-0.03709	0.03637	0.03935	8%	b_{1131}	0.17117	0.17440	0.16386	6%	b_{1131}	0	0	0	0	b_{1131}	0.03333	0.03311	-0.03333	1%	
b_{1132}	-0.05975	0.06042	0.05661	6%	b_{1132}	0	0	0	0	b_{1132}	0	0	0	0	b_{1132}	0.03343	-0.03378	-0.03594	6%	b_{1132}	0	0	0	0	
b_{1133}	0.08108	0.08206	0.08364	2%	b_{1133}	0	0	0	0	b_{1133}	0	0	0	0	b_{1133}	0.02667	0.02338	0.02339	0%	b_{1133}	0	0	0	0	
b_{1134}	0	0	0	0	b_{1134}	0.01119	-0.04193	-0.03948	6%	b_{1134}	0.02392	0.02267	0.02277	0%	b_{1134}	0	0	0	0	b_{1134}	0.02974	0.02990	-0.03152	5%	
b_{1135}	0.02190	0.02185	-0.02200	1%	b_{1135}	0	0	0	0	b_{1135}	0	0	0	0	b_{1135}	0.02999	0.03073	-0.02920	5%	b_{1135}	0	0	0	0	
b_{1141}	0.03791	0.03852	0.03868	0%	b_{1141}	0	0	0	0	b_{1141}	0	0	0	0	b_{1141}	0.08099	0.08163	0.07762	5%	b_{1141}	0	0	0	0	
b_{1142}	0	0	0	0	b_{1142}	-0.04796	-0.04733	-0.04364	8%	b_{1142}	0.22521	-0.23119	-0.24585	6%	b_{1142}	0	0	0	0	b_{1142}	-0.2136	0.02158	-0.20212	7%	
b_{1143}	0	0	0	0	b_{1143}	0.04655	-0.04697	-0.04411	6%	b_{1143}	0.01803	0.01631	0.01636	6%	b_{1143}	0	0	0	0	b_{1143}	0.02118	0.02148	-0.02031	5%	
b_{1144}	0.34088	0.34603	0.35002	1%	b_{1144}	0	0	0	0	b_{1144}	0	0	0	0	b_{1144}	0.04186	0.04112	0.04142	1%	b_{1144}	0	0	0	0	
b_{1151}	0	0	0	0	b_{1151}	-0.13952	0.13888	-0.14561	5%	b_{1151}	0.20255	0.21029	-0.19972	5%	b_{1151}	0	0	0	0	b_{1151}	0.03251	0.03196	0.03238	1%	
b_{1152}	-0.06222	0.06282	-0.06322	1%	b_{1152}	0	0	0	0	b_{1152}	0	0	0	0	b_{1152}	-0.03748	0.03783	-0.03525	7%	b_{1152}	0	0	0	0	
b_{1153}	0.02190	0.02185	-0.02200	1%	b_{1153}	0	0	0	0	b_{1153}	0	0	0	0	b_{1153}	-0.02560	-0.02558	-0.02360	8%	b_{1153}	0	0	0	0	
b_{1154}	0	0	0	0	b_{1154}	-0.06348	0.06273	-0.05827	7%	b_{1154}	0.35252	0.35857	-0.37768	5%	b_{1154}	0	0	0	0	b_{1154}	0.02982	0.02916	0.02949	1%	
b_{1155}	0.48408	0.49009	0.49626	1%	b_{1155}	0	0	0	0	b_{1155}	0	0	0	0	b_{1155}	0.05705	0.05601	0.05654	1%	b_{1155}	0	0	0	0	
b_{1221}	0.22357	0.22823	0.23092	1%	b_{1221}	0	0	0	0	b_{1221}	0	0	0	0	b_{1221}	-0.02560	-0.02558	-0.02360	8%	b_{1221}	0	0	0	0	
b_{1222}	0	0	0	0	b_{1222}	0.26634	0.27587	0.27403	1%	b_{1222}	0.06669	-0.07876	-0.07909	0%	b_{1222}	0	0	0	0	b_{1222}	-0.02111	0.02278	-0.02296	1%	
b_{1223}	0	0	0	0	b_{1223}	0.01850	-0.02129	-0.02139	0%	b_{1223}	0.26692	0.27435	0.27908	2%	b_{1223}	0	0	0	0	b_{1223}	-0.01844	0.01904	0.01800	5%	
b_{1224}	-0.09054	-0.09132	-0.08418	8%	b_{1224}	0	0	0	0	b_{1224}	0	0	0	0	b_{1224}	0.14102	0.14590	0.14725	1%	b_{1224}	0	0	0	0	
b_{1225}	0	0	0	0	b_{1225}	-0.06939	0.07388	-0.07438	1%	b_{1225}	0	-0.21859	-0.22834	0.21563	6%	b_{1225}	0	0	0	0	b_{1225}	0.04879	-0.04927	-0.05214	6%
b_{1231}	-0.07002	0.07018	0.07591	8%	b_{1231}	0	0	0	0	b_{1231}	0	0	0	0	b_{1231}	0.02199	0.02266	-0.02134	6%	b_{1231}	0	0	0	0	
b_{1232}	0	0	0	0	b_{1232}	-0.04796	-0.04733	-0.04364	8%	b_{1232}	0.16784	-0.17373	-0.16313	6%	b_{1232}	0	0	0	0	b_{1232}	-0.04244	0.04283	-0.04494	5%	
b_{1233}	0.06255	0.06291	-0.06338	1%	b_{1233}	0	0	0	0	b_{1233}	0	0	0	0	b_{1233}	-0.02975	0.03041	-0.03205	5%	b_{1233}	0	0	0	0	
b_{1234}	0.07878	-0.09062	-0.08509	6%	b_{1234}	0	0	0	0	b_{1234}	0.07402	0.07417	0.07547	2%	b_{1234}	0.06700	-0.00521	-0.00520	0%	b_{1234}	-0.00283	0.00235	-0.00237	1%	
b_{1235}	0	0	0	0	b_{1235}	-0.06062	-0.06173	-0.06581	6%	b_{1235}	0	-0.35269	-0.36471	0.38396	5%	b_{1235}	0	0	0	0	b_{1235}	0.07955	0.08253	0.07916	4%
b_{1236}	0	0	0	0	b_{1236}	-0.06062	-0.06173	-0.06581	6%	b_{1236}	0	-0.35351	-0.36283	-0.38244	2%	b_{1236}	0	0	0	0	b_{1236}	0.0144	-0.01866	-0.01201	1%
b_{1237}	0	0	0	0	b_{1237}	0.01850	-0.02129	-0.02139	0%	b_{1237}	0	0	0	0	b_{1237}	-0.01844	-0.01904	0.01800	5%	b_{1237}	0	0	0	0	
b_{1238}	0	0	0	0	b_{1238}	0.0101	0.0131	0.07697	5%	b_{1238}	0.00700	-0.00521	-0.00520	0%	b_{1238}	0	0	0	0	b_{1238}	-0.00385	0.00342	-0.00345	1%	
b_{1239}	-0.17252	-0.17588	-0.18602	6%	b_{1239}	0	0	0	0	b_{1239}	0	0	0	0	b_{1239}	0.09860	0.10277	0.09780	5%	b_{1239}	0	0	0	0	
b_{1243}	0.07775	-0.08090	-0.07615	6%	b_{1243}	0	0	0	0	b_{1243}	0	0	0	0	b_{1243}	0.01781	0.01853	-0.01868	1%	b_{1243}	0	0	0	0	
b_{1244}	0.01252	0.01182	0.01188	0%	b_{1244}	0	0	0	0	b_{1244}	0	0	0	0	b_{1244}	0.06741	0.06758	0.06429	5%	b_{1244}	0	0	0	0	
b_{1245}	0.18455	0.18703	-0.19700	5%	b_{1245}	0	0	0	0	b_{1245}	0.03475	-0.03502	-0.03525	1%	b_{1245}	0.14185	0.14250	0.14318	2%	b_{1245}	0	0	0	0	
b_{1251}	0.02190	0.02185	-0.02200	1%	b_{1251}	0	0	0	0	b_{1251}	0	0	0	0	b_{1251}	0.03716	0.03765	-0.03557	6%	b_{1251}	0	0	0	0	
b_{1252}	0	0	0	0	b_{1252}	-0.06062	-0.06173	-0.06581	6%	b_{1252}	0	-0.35351	-0.36283	-0.38444	2%	b_{1252}	0	0	0	0	b_{1252}	0.01144	-0.01866	-0.01201	1%
b_{1253}	0	0	0	0	b_{1253}	-0.12666	0.1107	-0.11118	1%	b_{1253}	0	0.16495	0.16646	-0.16606	0%	b_{1253}	0	0	0	0	b_{1253} </				

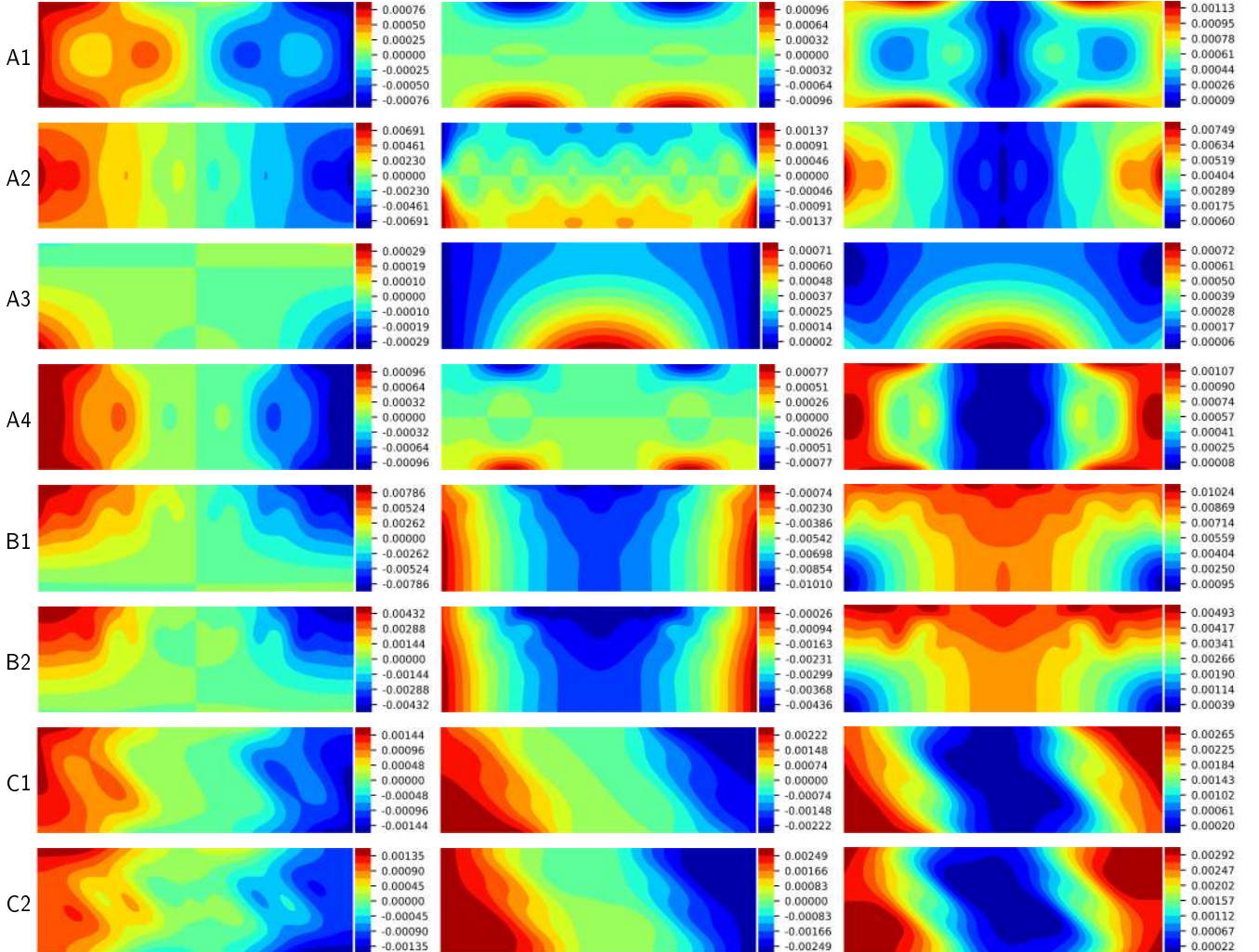


Figure 5: u_{33} for isotropic plate with $a/b = 3$; each row corresponds to one model; columns from left to right are: u , v , $\sqrt{u^2 + v^2}$

127.62900 GPa, $E_{22} = 11.30740$ GPa, $G_{12} = G_{23} = G_{13} = 6.00257$ GPa and $\nu_{12} = 0.300235$. Results using DIANA's CQ40L and Allman-type elements are present together with the BFSC results. The error of the BFSC implementation is again calculated about the results obtained with the Allman-type element. The same mesh, load and boundary conditions of the previous isotropic case are used. Again, a maximum error of 9% is verified for the b_{ijkl} coefficients, attributed to the differences in λ_i values between the Allman-type and BFSC elements.

Figure 8 illustrates the second-order field modes u_{ij} for the composite plate used in the multi-modal asymptotic expansion.

10. Conclusion

A complete displacement-based formulation for the Koiter's multi-modal asymptotic expansion was presented. The formulation and notation adopted enabled a close correspondence between the formulation and implemented algorithms, facilitating further developments on the field of initial post-

Table 8

Eigenvalues λ_i for composite plate used in multi-modal analysis, units in [N/m]

Eigenvalue	DIANA CQ40L	DIANA Allman	BFSC
λ_1	5257	5312	5303
λ_2	5420	5483	5467
λ_3	6011	6088	6060
λ_4	6132	6185	6178
λ_5	6877	6976	6928
λ_6	7967	8100	8021
λ_7	9258	9441	9317
λ_8	10740	10993	10804

buckling analysis and reduced-order models based on Koiter's method. The present work used state-of-the-art collaborative tools to implement the developed methods: Python [61], NumPy [62] and Cython [63].

A modified Bogner-Fox-Schmit (BFS) finite element

Table 9Multi-modal expansion coefficients b_{ijkl} for composite plate using 5 modes

b_{ijkl}	DIANA CQ40L	DIANA Allm n	BFSC	Err	b_{ijkl}	DIANA CQ40L	DIANA Allm n	BFSC	Err	b_{ijkl}	DIANA CQ40L	DIANA Allm n	BFSC	Err	b_{ijkl}	DIANA CQ40L	DIANA Allm n	BFSC	Err
b_{1111}	0.18993	0.18860	0.18646	1%	b_{2111}	0	0	0	0	b_{3111}	-0.01064	-0.01116	0.01117	0%	b_{4111}	0	0	0	0
b_{1112}	0	0	0	0	b_{2112}	0.10871	0.10467	0.10615	1%	b_{3112}	0	0	0	0	b_{4112}	0.10064	0.09356	0.08835	6%
b_{1113}	-0.03384	-0.03531	0.05531	0%	b_{2113}	0	0	0	0	b_{3113}	0.09543	0.09339	0.09447	1%	b_{4113}	0	0	0	0
b_{1114}	0	0	0	0	b_{2114}	0.02851	0.02771	0.02604	6%	b_{3114}	0	0	0	0	b_{4114}	0.13833	0.13851	0.14054	1%
b_{1115}	0	0	0	0	b_{2115}	-0.02944	-0.02877	0.02901	1%	b_{3115}	0	0	0	0	b_{4115}	-0.03644	-0.03392	0.03449	1%
b_{1121}	0	0	0	0	b_{2121}	0.09250	0.08810	0.08345	5%	b_{3121}	0	0	0	0	b_{4121}	0.10381	0.10497	0.10425	8%
b_{1131}	0.19800	0.18567	0.18169	2%	b_{2131}	0.02464	0.02214	0.02063	7%	b_{3131}	0.02464	0.02124	0.02063	7%	b_{4131}	0	0	0	0
b_{1132}	0	0	0	0	b_{2132}	0.08446	0.08087	-0.08539	6%	b_{3132}	0	0	0	0	b_{4132}	0.13451	0.13344	-0.12660	5%
b_{1134}	0.05216	0.04922	0.04641	6%	b_{2134}	0	0	0	0	b_{3134}	0.02454	0.02422	-0.02281	6%	b_{4134}	0	0	0	0
b_{1135}	-0.05306	-0.05109	0.05169	1%	b_{2135}	0	0	0	0	b_{3135}	0.07375	0.06968	0.07309	5%	b_{4135}	0	0	0	0
b_{1141}	-0.03384	-0.03531	0.05531	0%	b_{2141}	0	0	0	0	b_{3141}	0.07951	0.07781	0.07424	0	b_{4141}	0	0	0	0
b_{1142}	0.05216	0.04922	0.04641	6%	b_{2142}	0	0	0	0	b_{3142}	0.03322	0.03282	-0.03470	6%	b_{4142}	0	0	0	0
b_{1144}	0.07169	0.07286	0.07382	1%	b_{2144}	0	0	0	0	b_{3144}	-0.00231	-0.00184	0.00188	2%	b_{4144}	0	0	0	0
b_{1145}	-0.01888	-0.01784	0.01790	0%	b_{2145}	0	0	0	0	b_{3145}	0.02959	0.03017	0.02878	5%	b_{4145}	0	0	0	0
b_{1151}	0	0	0	0	b_{2151}	-0.02964	-0.02832	0.02838	0%	b_{3151}	0	0	0	0	b_{4151}	-0.03360	-0.03137	0.03199	2%
b_{1152}	-0.05386	-0.05109	0.05169	1%	b_{2152}	0	0	0	0	b_{3152}	0.03659	0.03461	0.03273	5%	b_{4152}	0	0	0	0
b_{1153}	0	0	0	0	b_{2153}	0.05671	0.05304	0.04936	7%	b_{3153}	0	0	0	0	b_{4153}	0.31573	0.30416	0.31875	5%
b_{1154}	-0.01888	-0.01784	0.01790	0%	b_{2154}	0	0	0	0	b_{3154}	0.03635	0.03617	0.03431	4%	b_{4154}	0	0	0	0
b_{1155}	0.42279	0.40110	0.40683	1%	b_{2155}	0	0	0	0	b_{3155}	-0.05338	-0.04528	0.04646	3%	b_{4155}	0	0	0	0
b_{1211}	0	0	0	0	b_{2111}	0.10871	0.10467	0.10615	1%	b_{3111}	0	0	0	0	b_{4111}	0.10064	0.09356	0.08835	6%
b_{1212}	0.16924	0.15646	0.14871	5%	b_{2112}	0	0	0	0	b_{3112}	0.04859	0.04539	-0.04519	6%	b_{4112}	0	0	0	0
b_{1213}	0	0	0	0	b_{2113}	0.04284	0.03944	-0.03659	7%	b_{3113}	0	0	0	0	b_{4113}	0.15060	0.14565	-0.13722	6%
b_{1214}	0.06157	0.05785	0.06264	8%	b_{2114}	0	0	0	0	b_{3114}	0.02192	0.02219	-0.02104	5%	b_{4114}	0	0	0	0
b_{1215}	-0.05423	-0.05030	0.05057	1%	b_{2115}	0	0	0	0	b_{3115}	0.03262	0.02977	0.02784	6%	b_{4115}	0	0	0	0
b_{1221}	0.19890	0.18567	0.18196	2%	b_{2121}	0	0	0	0	b_{3121}	0.02464	0.02214	-0.02063	7%	b_{4121}	0	0	0	0
b_{1222}	0	0	0	0	b_{2122}	0.25341	0.24575	0.24462	0%	b_{3122}	0	0	0	0	b_{4122}	-0.06973	-0.08089	-0.07988	1%
b_{1223}	0.07839	0.07004	-0.06520	7%	b_{2123}	0	0	0	0	b_{3123}	0.14389	0.13969	0.14099	1%	b_{4123}	0	0	0	0
b_{1224}	0	0	0	0	b_{2124}	-0.01975	-0.02396	-0.02355	2%	b_{3124}	0	0	0	0	b_{4124}	0.23989	0.22601	0.23077	2%
b_{1225}	0	0	0	0	b_{2125}	-0.06766	-0.07177	0.07160	0%	b_{3125}	0	0	0	0	b_{4125}	0.19737	0.18845	-0.17989	5%
b_{1231}	0.15454	0.14361	-0.15261	6%	b_{2131}	0	0	0	0	b_{3131}	0.01056	0.00946	0.00952	4%	b_{4131}	0	0	0	0
b_{1233}	0	0	0	0	b_{2133}	0.25015	0.24887	0.25000	0%	b_{3133}	0	0	0	0	b_{4133}	-0.11461	-0.10795	-0.10874	1%
b_{1234}	0.06971	0.07019	-0.06650	5%	b_{2134}	0	0	0	0	b_{3134}	-0.01857	-0.01900	-0.01911	1%	b_{4134}	0	0	0	0
b_{1235}	0.03736	0.03942	0.03879	7%	b_{2135}	0	0	0	0	b_{3135}	0.10470	0.10182	-0.10542	4%	b_{4135}	0	0	0	0
b_{1241}	0.05216	0.04922	0.04641	6%	b_{2141}	0	0	0	0	b_{3141}	0.03332	0.03282	-0.03470	6%	b_{4141}	0	0	0	0
b_{1242}	0	0	0	0	b_{2142}	-0.01975	-0.02396	-0.02355	2%	b_{3142}	0	0	0	0	b_{4142}	0.02456	0.02456	0.02342	5%
b_{1243}	0.07805	0.07661	-0.07208	6%	b_{2143}	0.06795	0.06695	0.06802	2%	b_{3143}	-0.01867	-0.01795	-0.01808	1%	b_{4143}	0	0	0	0
b_{1244}	0	0	0	0	b_{2144}	0.05590	0.05362	-0.05302	5%	b_{3144}	0	0	0	0	b_{4144}	-0.03351	-0.03217	0.02485	7%
b_{1245}	-0.05386	-0.05109	0.05169	1%	b_{2145}	0	0	0	0	b_{3145}	0.03659	0.03461	0.03273	5%	b_{4145}	0	0	0	0
b_{1251}	0	0	0	0	b_{2151}	-0.06766	-0.07177	0.07160	0%	b_{3151}	0	0	0	0	b_{4151}	0.32196	0.30442	-0.31968	5%
b_{1252}	0.23458	0.22045	0.23094	5%	b_{2152}	0	0	0	0	b_{3152}	0.03422	0.03612	-0.03311	8%	b_{4152}	0	0	0	0
b_{1254}	0	0	0	0	b_{2154}	0.05590	0.05582	-0.05302	5%	b_{3154}	-0.03637	-0.03426	0.03111	8%	b_{4154}	-0.03637	-0.03426	0.03111	8%
b_{1255}	0	0	0	0	b_{2155}	0.35028	0.33699	0.34263	1%	b_{3155}	0	0	0	0	b_{4155}	-0.14729	-0.13501	-0.13719	2%
b_{1256}	0.09411	0.09544	0.09092	5%	b_{2156}	0	0	0	0	b_{3156}	-0.02607	-0.02237	0.02292	2%	b_{4156}	0	0	0	0
b_{1257}	-0.09736	-0.09582	0.09594	2%	b_{2157}	0	0	0	0	b_{3157}	0.29010	0.27197	0.27501	1%	b_{4157}	0	0	0	0
b_{1258}	0.11564	0.11445	0.10841	5%	b_{2158}	0.02771	0.02604	0.02219	7%	b_{3158}	0.01056	0.00946	0.00916	4%	b_{4158}	-0.01420	-0.01106	0.01132	2%
b_{1259}	0.07084	0.08042	0.07584	6%	b_{2159}	0.05792	0.05846	-0.06152	5%	b_{3159}	0	0	0	0	b_{4159}	0.01828	0.01915	0.01822	5%
b_{1261}	-0.01741	-0.01650	0.01680	2%	b_{2161}	0	0	0	0	b_{3161}	0.05792	0.05846	-0.06152	5%	b_{4161}	0	0	0	0
b_{1262}	0.05166	0.04922	0.04641	6%	b_{2162}	0	0	0	0	b_{3162}	0.02454	0.02422	-0.02281	6%	b_{4162}	0	0	0	0
b_{1263}	-0.01788	-0.01784	0.01790	0%	b_{2163}	-0.01975	-0.02396	-0.02355	2%	b_{3163}	0	0	0	0	b_{4163}	0.23989	0.22601	0.23077	2%
b_{1264}	0	0	0	0	b_{2164}	-0.03246	-0.03198	-0.03205	0%	b_{3164}	-0.01867	-0.01795	-0.01808	1%	b_{4164}	0	0	0	0
b_{1265}	-0.01043	-0.00991	0.00998	4%	b_{2165}	0	0	0	0	b_{3165}	0.05953	0.06552	0.06251	5%	b_{4165}	0	0	0	0
b_{1266}	0.16363	0.16000	0.16743	5%	b_{2166}	0	0	0	0	b_{3166}	-0.02759	-0.02156	0.02216	3%	b_{4166}	0	0	0	0
b_{1267}	0.07169	0.07286	0.07382	1%	b_{2167}	0	0	0	0	b_{3167}	-0.02023	-0.01804	0.01881	2%	b_{4167}	0	0	0	0
b_{1268}	0	0	0	0	b_{2168}	0.06795	0.06695	0.06802	2%	b_{3168}	0	0	0	0	b_{4168}	-0.03673	-0.03427	0.03075	2%
b_{1269}	-0.00736	-0.00582	0.00594	2%	b_{2169}	0	0	0	0	b_{3169}	0.06091	0.06062	0.06154	2%	b_{4169}	0	0</td		

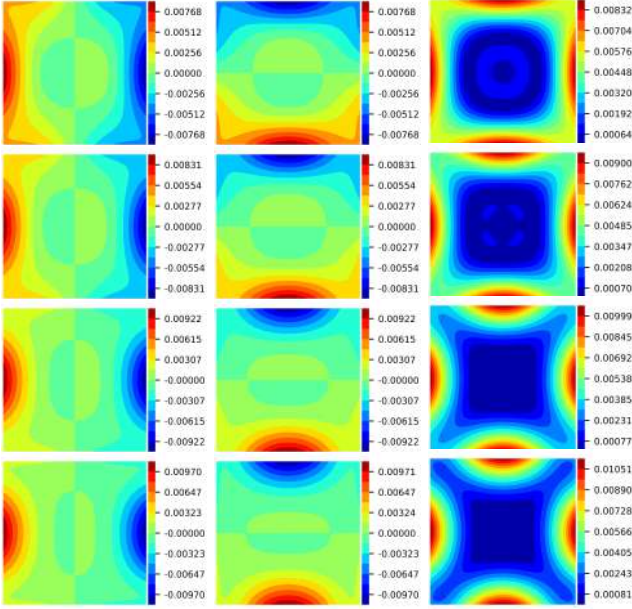


Figure 6: u_{11} for anisotropic plate A1 with $a/b = 1$; rows from top to bottom are: $E_1/E_2 = 1, 3, 10, 20$; columns from left to right are: $u, v, \sqrt{u^2 + v^2}$

was proposed and referred to as Bogner-Fox-Schmidt-Castro (BFSC), which has enriched in-place displacements when compared to the conventional BFS element to enable an accurate representation of the second-order displacement fields. This element has only 4 nodes per element and 10 degrees-of-freedom per node, which are: $u, u_x, u_y, v, v_x, v_y, w, w_x, w_y$ and w_{xy} . The results herein presented showed that the third-order interpolation of w provided led to an ultra-fast convergence of the linear buckling eigenvalues, whereas the third-order interpolation of u and v led to a ultra-fast convergence of the second-order displacement fields and consequently of the b_{ijkl} factors obtained in Koiter's analysis.

Future studies should investigate the same strategy herein adopted to enrich the in-plane interpolation of the BFS element to create modified versions of the TUBA3 family [57]. Other approaches for enriching the membrane displacement field could also be investigated, such as the interpolation covers suggested by Jun et al. [71] for triangular shell elements. Another alternative is to use fifth-order Hermite polynomials enhancing the BFS element to also interpolate the rotational strains w_{xx} and w_{yy} , keeping C^1 continuity even with distorted meshes, thus keeping the high convergence rates herein observed for non-rectangular meshes [72].

In the present study, Von Kármán nonlinear kinematics were used to derive the n^{th} -order tensors obtained from the total potential energy of the system. The effect of using more complete nonlinear kinematics such as Sanders [49, 52] and Timoshenko & Gere [52] should also be investigated, especially for shells with single and double curvature.

The displacement-based notation herein presented simplifies formulating and implementing the compatibility be-

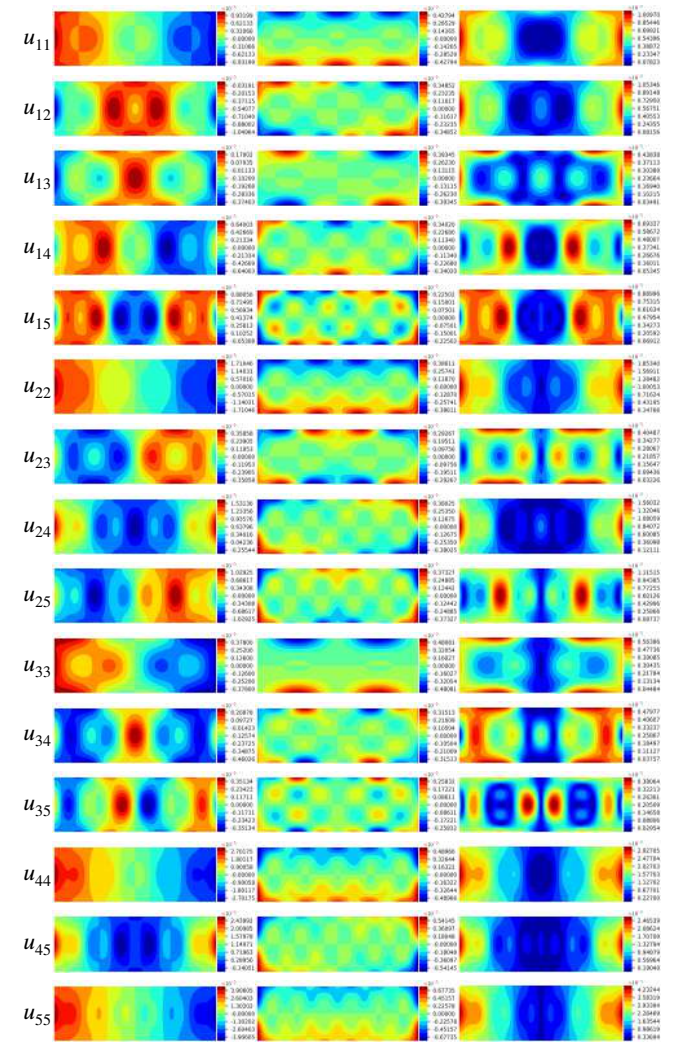


Figure 7: u_{ij} for isotropic plate used in multi-modal asymptotic expansion analysis; columns from left to right are: $u, v, \sqrt{u^2 + v^2}$

tween different semi-analytical domains [73, 74, 75, 76], even for Koiter's asymptotic analysis. Such possibilities would allow one to apply semi-analytical methods for stiffened panels and shells using efficient displacement representations such as those provided by Legendre hierarchical polynomials [77, 78, 79, 80].

Finally, the effect of initial imperfections should be included in the presented formulation to enable asymptotic perturbation analyses, especially important in imperfection sensitive shells.

CRediT authorship contribution statement

S. G. P. Castro: Conceptualization, methodology, formal analysis, investigation, validation, software, data curation, writing - original draft preparation, writing - editing. **E. L. Jansen:** Validation, writing - review.

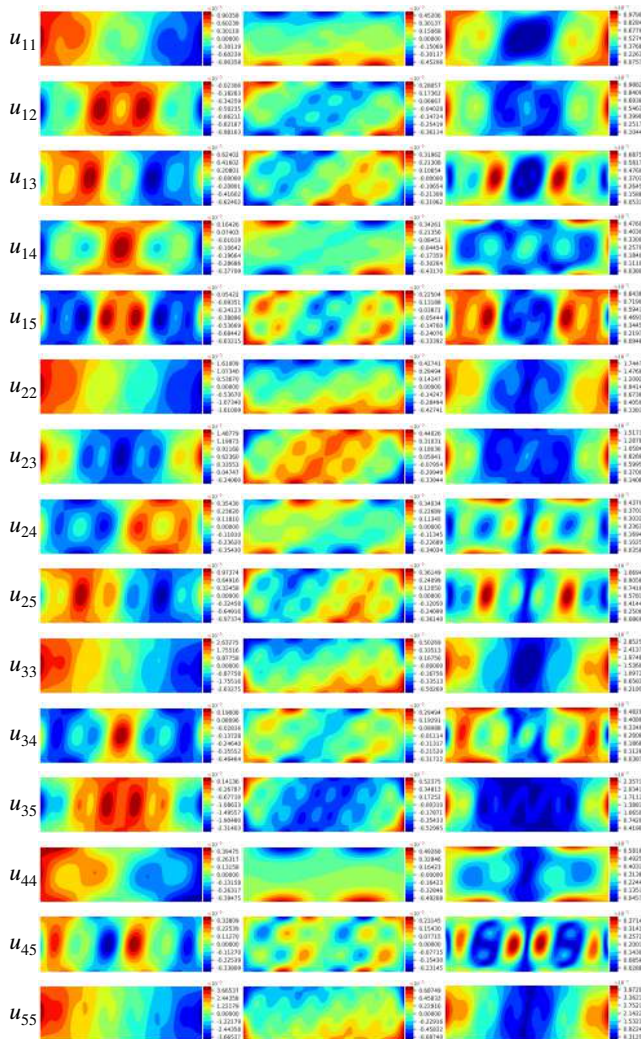


Figure 8: \mathbf{u}_{ij} for composite plate used in multi-modal asymptotic expansion analysis; columns from left to right are: u , v , $\sqrt{u^2 + v^2}$

A. Linear Buckling Analysis

In Eq. 5 it is known from the equilibrium condition that $\phi'[\mathbf{u}_c, \lambda_c] = 0$. Dividing the remaining terms by $\|\mathbf{v}\|$:

$$\begin{aligned} \phi'[\mathbf{u}, \lambda_c]\delta\mathbf{u} &= \phi''[\mathbf{u}_c, \lambda_c]\frac{\mathbf{v}}{\|\mathbf{v}\|}\delta\mathbf{u} + \frac{1}{2}\phi'''[\mathbf{u}_c, \lambda_c]\mathbf{v}^2\frac{1}{\|\mathbf{v}\|}\delta\mathbf{u} \\ &\quad + \frac{1}{6}\phi^{iv}[\mathbf{u}_c, \lambda_c]\mathbf{v}^3\frac{1}{\|\mathbf{v}\|}\delta\mathbf{u} + O(4) = 0 \end{aligned} \quad (58)$$

It becomes convenient to define a normalized eigenvector \mathbf{u}_i at $\lambda \rightarrow \lambda_i$, such that $\langle \mathbf{u}_i, \mathbf{u}_i \rangle = 1$:

$$\mathbf{u}_i = \frac{\mathbf{v}}{\|\mathbf{v}\|} \quad (59)$$

Thus, one can change Eq. 58 using the definition of \mathbf{u}_i to obtain:

$$\begin{aligned} \phi'[\mathbf{u}, \lambda_i]\delta\mathbf{u} &= \phi''[\mathbf{u}_c, \lambda_i]\mathbf{u}_i\delta\mathbf{u} + \frac{1}{2}\phi'''[\mathbf{u}_c, \lambda_i]\mathbf{u}_i\mathbf{v}^2\delta\mathbf{u} \\ &\quad + \frac{1}{6}\phi^{iv}[\mathbf{u}_c, \lambda_i]\mathbf{u}_i\mathbf{v}^2\delta\mathbf{u} + O(4) = 0 \end{aligned} \quad (60)$$

From Eq. 60, the following relation is obtained when $\lambda \rightarrow \lambda_i$, i.e. $\mathbf{v} \rightarrow \mathbf{0}$:

$$\phi''[\mathbf{u}_c, \lambda_i]\mathbf{u}_i\delta\mathbf{u} = \phi''[\lambda_i\mathbf{u}_0, \lambda_i]\mathbf{u}_i\delta\mathbf{u} = 0 \quad (61)$$

Equation 61 represents the Neutral Equilibrium Criterion [29], which can be used to compute λ_i and \mathbf{u}_i , i.e. the linear buckling eigenvalues and eigenmodes, based on a pre-buckling state $[\mathbf{u}_0, \lambda_0]$. For a system with N degrees-of-freedom there are N pairs λ_i, \mathbf{u}_i , so that one should select the mode \mathbf{u}_i that corresponds to the lowest positive λ_i , named λ_c in the previous discussions for single-mode asymptotic expansion. In most commonly used eigenvalue solvers, the eigenvalues can be computed and sorted in ascendant order, such that only a few first pairs of eigenvalues and eigenvectors need to be calculated.

References

- [1] W. T. Koiter, The Stability of Elastic Equilibrium, Ph.D. thesis, Translation by Eduard Riks, Technical Report AFFDL-TR-70-25, February 1970. Delft University of Technology (1945).
- [2] G. A. Cohen, Effect of a nonlinear prebuckling state on the postbuckling behavior and imperfection sensitivity of elastic structures., AIAA Journal 6 (8) (1968) 1616–1619. doi:10.2514/3.4832. URL <https://arc.aiaa.org/doi/10.2514/3.4832>
- [3] J. Arboz, J. Hol, Koiter's stability theory in a computer-aided engineering (CAE) environment, International Journal of Solids and Structures 26 (9-10) (1990) 945–973. doi:10.1016/0020-7683(90)90011-J. URL <https://linkinghub.elsevier.com/retrieve/pii/00207683900011J>
- [4] J. F. Olesen, E. Byskov, Accurate determination of asymptotic post-buckling stresses by the finite element method, Computers & Structures 15 (2) (1982) 157–163. doi:10.1016/0045-7949(82)90063-3. URL <https://linkinghub.elsevier.com/retrieve/pii/0045794982900633>
- [5] R. Peek, M. Kheykhahan, Postbuckling behavior and imperfection sensitivity of elastic structures by the Lyapunov-Schmidt-Koiter approach, Computer Methods in Applied Mechanics and Engineering 108 (3-4) (1993) 261–279. doi:10.1016/0045-7825(93)90005-I. URL <https://linkinghub.elsevier.com/retrieve/pii/004578259390005I>
- [6] C. Menken, G. Schreppers, W. Groot, R. Petterson, Analyzing buckling mode interactions in elastic structures using an asymptotic approach; theory and experiments, Computers & Structures 64 (1-4) (1997) 473–480. doi:10.1016/S0045-7949(96)00139-3. URL <https://linkinghub.elsevier.com/retrieve/pii/S0045794996001393>
- [7] R. Casciaro, G. Garcea, G. Attanasio, F. Giordano, Perturbation approach to elastic post-buckling analysis, Computers & Structures 66 (5) (1998) 585–595. doi:10.1016/S0045-7949(97)00112-0. URL <https://linkinghub.elsevier.com/retrieve/pii/S0045794997001120>
- [8] M. Kheykhahan, R. Peek, Postbuckling analysis and imperfection sensitivity of general shells by the finite element method, International Journal of Solids and Structures 36 (18) (1999) 2641–2681.

- doi:10.1016/S0020-7683(98)00129-2.
 URL <https://linkinghub.elsevier.com/retrieve/pii/S0020768398001292>
- [9] R. Casciaro, Computational asymptotic post-buckling analysis of slender elastic structures, in: *Phenomenological and Mathematical Modelling of Structural Instabilities*, Vol. 470, Springer Vienna, Vienna, 2005, pp. 195–276. doi:10.1007/3-211-38028-0_4.
 URL http://link.springer.com/10.1007/3-211-38028-0_4
- [10] P. Tiso, M. M. Abdalla, E. L. Jansen, Koiter's post-buckling analysis of general shell structures using the finite element method, in: *ICAS-Secretariat - 25th Congress of the International Council of the Aeronautical Sciences 2006*, 2006.
- [11] P. Tiso, Finite element based reduction methods for static and dynamic analysis of thin-walled structures, Doctoral thesis, Delft University of Technology (2006).
 URL <https://repository.tudelft.nl/islandora/object/uuid%3A3affd8eb-8fdb-40da-aefc-48a96efe8afb?collection=research>
- [12] T. Rahman, E. Jansen, Finite element based coupled mode initial post-buckling analysis of a composite cylindrical shell, *Thin-Walled Structures* 48 (1) (2010) 25–32. doi:10.1016/j.tws.2009.08.003.
 URL <https://www.sciencedirect.com/science/article/pii/S0263823109001608>
- [13] T. Rahman, E. L. Jansen, Finite element based coupled mode initial post-buckling analysis of a composite cylindrical shell, *Thin-Walled Structures* 48 (1) (2010) 25–32. doi:10.1016/j.tws.2009.08.003.
 URL <http://linkinghub.elsevier.com/retrieve/pii/S0263823109001608>
- [14] T. Rahman, S. T. Ijsselmuiden, M. M. Abdalla, E. L. Jansen, Postbuckling analysis of variable stiffness composite plates using a finite element-based perturbation method, *International Journal of Structural Stability and Dynamics* 11 (04) (2011) 735–753. doi:10.1142/S0219455411004324.
 URL <https://www.worldscientific.com/doi/abs/10.1142/S0219455411004324>
- [15] S. R. Henrichsen, P. M. Weaver, E. Lindgaard, E. Lund, Post-buckling optimization of composite structures using Koiter's method, *International Journal for Numerical Methods in Engineering* 108 (8) (2016) 902–940. doi:10.1002/nme.5239.
 URL <http://doi.wiley.com/10.1002/nme.5239>
- [16] A. Madeo, R. M. Groh, G. Zucco, P. M. Weaver, G. Zagari, R. Zinno, Post-buckling analysis of variable-angle tow composite plates using Koiter's approach and the finite element method, *Thin-Walled Structures* 110 (2017) 1–13. doi:10.1016/j.tws.2016.10.012.
- [17] S. White, G. Raju, P. Weaver, Initial post-buckling of variable-stiffness curved panels, *Journal of the Mechanics and Physics of Solids* 71 (1) (2014) 132–155. doi:10.1016/j.jmps.2014.07.003.
 URL <https://linkinghub.elsevier.com/retrieve/pii/S0022509614001410>
- [18] G. Raju, S. White, Z. Wu, P. Weaver, Optimal Postbuckling Design of Variable Angle Tow Composites using Lamination Parameters, in: *56th AIAA/ASCE/AHS/ASC Structures, Structural Dynamics, and Materials Conference*, 2015. doi:10.2514/6.2015-0451.
 URL <http://arc.aiaa.org/doi/10.2514/6.2015-0451>
- [19] F. S. Liguori, G. Zucco, A. Madeo, D. Magisano, L. Leonetti, G. Garcea, P. M. Weaver, Postbuckling optimisation of a variable angle tow composite wingbox using a multi-modal Koiter approach, *Thin-Walled Structures* 138 (2019) 183–198. doi:10.1016/j.tws.2019.01.035.
 URL <https://linkinghub.elsevier.com/retrieve/pii/S0263823118316331>
- [20] F. S. Liguori, G. Zucco, A. Madeo, D. Magisano, L. Leonetti, G. Garcea, P. M. Weaver, Koiter method and solid shell finite elements for postbuckling optimisation of variable angle tow composite structures, in: A. Carcaterra, A. Paolone, G. Graziani (Eds.), *Proceedings of XXIV AIMETA Conference 2019*, Springer International Publishing, Cham, 2020, pp. 1731–1742.
- [21] E. J. Barbero, A. Madeo, G. Zagari, R. Zinno, G. Zucco, Imperfec-
- tion sensitivity analysis of composite cylindrical shells using Koiter's method, *International Journal for Computational Methods in Engineering Science and Mechanics* 18 (1) (2017) 105–111. doi:10.1080/15502287.2016.1276359.
 URL <https://www.tandfonline.com/doi/full/10.1080/15502287.2016.1276359>
- [22] E. Jansen, T. Rahman, R. Rolfs, Finite element integrated fast buckling analysis tools using a perturbation approach, in: *Buckling and Postbuckling Structures II: Experimental, Analytical and Numerical Studies*, 2018. doi:10.1142/9781786344335_0005.
- [23] Y. Sun, K. Tian, R. Li, B. Wang, Accelerated Koiter method for post-buckling analysis of thin-walled shells under axial compression, *Thin-Walled Structures* 155 (2020) 106962. doi:10.1016/j.tws.2020.106962.
 URL <https://linkinghub.elsevier.com/retrieve/pii/S0263823120308405>
- [24] W. Rissardo, Uma metodologia de pre-dimensionamento para estabilidade estrutural de asas, *Dissertacao de Mestrado*, Ph.D. thesis, Instituto Tecnologico de Aeronautica, Sao Jose dos Campos, Brasil (2006).
- [25] G. C. Bufeli, A. Teixeira Neto, F. L. d. S. Bussamra, A routine to generate a simplified dynamic model of wing main box, in: *Brazilian Symposium on Aerospace Engineering & Applications*, Sao Jose dos Campos, Brazil, 2009.
- [26] A. Teixeira Neto, F. L. d. S. Bussamra, H. A. d. C. e. Silva, A new metamodel for reinforced panels under compressive loads and its application to the fuselage conception, *Latin American Journal of Solids and Structures* 11 (2) (2014) 223–244.
- [27] S. G. Castro, R. Zimmermann, M. A. Arbelo, R. Degenhardt, Exploring the constancy of the global buckling load after a critical geometric imperfection level in thin-walled cylindrical shells for less conservative knock-down factors, *Thin-Walled Structures* 72 (2013) 76–87. doi:10.1016/j.tws.2013.06.016.
- [28] S. G. Castro, R. Zimmermann, M. A. Arbelo, R. Khakimova, M. W. Hilburger, R. Degenhardt, Geometric imperfections and lower-bound methods used to calculate knock-down factors for axially compressed composite cylindrical shells, *Thin-Walled Structures* 74 (2014) 118–132. doi:10.1016/j.tws.2013.08.011.
- [29] S. G. Castro, C. Mittelstedt, F. A. Monteiro, M. A. Arbelo, G. Ziegmann, R. Degenhardt, Linear buckling predictions of unstiffened laminated composite cylinders and cones under various loading and boundary conditions using semi-analytical models, *Composite Structures* 118 (1) (2014) 303–315. doi:10.1016/j.compstruct.2014.07.037.
 URL <http://dx.doi.org/10.1016/j.compstruct.2014.07.037>
- [30] S. G. Castro, C. Mittelstedt, F. A. Monteiro, M. A. Arbelo, R. Degenhardt, G. Ziegmann, A semi-analytical approach for linear and non-linear analysis of unstiffened laminated composite cylinders and cones under axial, torsion and pressure loads, *Thin-Walled Structures* 90 (2015) 61–73. doi:10.1016/j.tws.2015.01.002.
 URL <http://dx.doi.org/10.1016/j.tws.2015.01.002>
- [31] S. G. P. Castro, C. Mittelstedt, F. A. C. Monteiro, R. Degenhardt, G. Ziegmann, Evaluation of non-linear buckling loads of geometrically imperfect composite cylinders and cones with the Ritz method, *Composite Structures* 122 (2015) 284–299. doi:10.1016/j.compstruct.2014.11.050.
 URL <http://dx.doi.org/10.1016/j.compstruct.2014.11.050>
- [32] E. J. Barbero, A. Madeo, G. Zagari, R. Zinno, G. Zucco, Imperfection sensitivity analysis of laminated folded plates, *Thin-Walled Structures* 90 (2015) 128–139. doi:10.1016/j.tws.2015.01.017.
 URL <http://dx.doi.org/10.1016/j.tws.2015.01.017>
<https://linkinghub.elsevier.com/retrieve/pii/S0263823115000208>
- [33] R. M. Groh, A. Pirrera, Spatial chaos as a governing factor for imperfection sensitivity in shell buckling, *Physical Review E* 100 (3) (sep 2019). doi:10.1103/PhysRevE.100.032205.
- [34] J. Xia, P. E. Farrell, S. G. Castro, Nonlinear bifurcation analysis of stiffener profiles via deflation techniques, *Thin-Walled Structures* 149 (2020) 106662. doi:10.1016/j.tws.2020.106662.
 URL <https://linkinghub.elsevier.com/retrieve/pii/>

- S0263823119316404
- [35] E. Barbero, A. Madeo, G. Zagari, R. Zinno, G. Zucco, A mixed isostatic 24 dof element for static and buckling analysis of laminated folded plates, *Composite Structures* 116 (2014) 223–234. doi:10.1016/j.compstruct.2014.05.003.
- URL <https://linkinghub.elsevier.com/retrieve/pii/S026382314002037>
- [36] A. Madeo, G. Zagari, R. Casciaro, S. De Miranda, A mixed 4-node 3D plate element based on self-equilibrated isostatic stresses, *International Journal of Structural Stability and Dynamics* 15 (4) (may 2015). doi:10.1142/S0219455414500667.
- [37] G. Zucco, R. M. Groh, A. Madeo, P. M. Weaver, Mixed shell element for static and buckling analysis of variable angle tow composite plates, *Composite Structures* 152 (2016) 324–338. doi:10.1016/j.compstruct.2016.05.030.
- [38] B. Budiansky, Theory of Buckling and Post-Buckling Behavior of Elastic Structures, *Advances in Applied Mechanics* 14 (1974) 1–65. doi:10.1016/S0065-2156(08)70030-9.
- URL <https://linkinghub.elsevier.com/retrieve/pii/S0065215608700309>
- [39] F. K. Bogner, R. L. Fox, L. A. Schmit Jr., The generation of inter-element-compatible stiffness and mass matrices by the use of interpolation formulas, in: *Matrix Methods in Structural Mechanics*, Air-Force Inst. of Tech., Wright Patterson AF Base, Cleveland, Ohio, 1966, pp. 395–444.
- URL <http://contrails.iit.edu/reports/8569>
- [40] O. C. Zienkiewicz, R. L. Taylor, *The Finite Element Method Volume 2: Solid Mechanics*, fifth edit Edition, 2000.
- [41] K. Liang, M. Abdalla, G. Zafer, Q. Sun, A Koiter-Newton Approach for Nonlinear Structural Analysis, in: *3rd Aircraft Structural Design Conference*, 2012, p. 9.
- [42] K. Liang, M. Ruess, M. Abdalla, The Koiter-Newton approach using von Kármán kinematics for buckling analyses of imperfection sensitive structures, *Computer Methods in Applied Mechanics and Engineering* 279 (2014) 440–468. doi:10.1016/j.cma.2014.07.008.
- [43] K. Liang, M. Ruess, M. Abdalla, An eigenanalysis-based bifurcation indicator proposed in the framework of a reduced-order modeling technique for non-linear structural analysis, *International Journal of Non-Linear Mechanics* 81 (2016) 129–138. doi:10.1016/j.ijnonlinmec.2016.01.013.
- [44] K. Liang, Koiter-Newton analysis of thick and thin laminated composite plates using a robust shell element, *Composite Structures* 161 (2017) 530–539. doi:10.1016/j.compstruct.2016.10.071.
- [45] G. B. Arfken, H. J. Weber, D. Spector, *Mathematical Methods for Physicists*, 4th ed., American Journal of Physics 67 (2) (1999) 165–169. doi:10.1119/1.19217.
- URL <http://aapt.scitation.org/doi/10.1119/1.19217>
- [46] P. Tiso, E. Jansen, M. Abdalla, Reduction Method for Finite Element Nonlinear Dynamic Analysis of Shells, *AIAA Journal* 49 (10) (2011) 2295–2304. doi:10.2514/1.J051003.
- URL <http://arc.aiaa.org/http://arc.aiaa.org/doi/10.2514/1.J051003>
- [47] R. V. Southwell, On the General Theory of Elastic Stability, *Philosophical Transactions of the Royal Society A: Mathematical, Physical and Engineering Sciences* 213 (497–508) (1914) 187–244. doi:10.1088/rsta.1914.0005.
- URL <http://rsta.royalsocietypublishing.org/cgi/doi/10.1088/rsta.1914.0005>
- [48] C. Hühne, R. Zimmermann, R. Rolfs, B. M. Geier, Sensitivities to geometrical and loading imperfections on buckling of composite cylindrical shells, in: *Proceedings European Conference on Spacecraft Structures, Materials and Mechanical Testing*, Toulouse, France, 2002, p. 12.
- [49] S. G. Castro, C. Mittelstedt, F. A. Monteiro, M. A. Arbelo, G. Ziegmann, R. Degenhardt, Linear buckling predictions of unstiffened laminated composite cylinders and cones under various loading and boundary conditions using semi-analytical models, *Composite Structures* 118 (1) (2014) 303–315. doi:10.1016/j.compstruct.2014.07.037.
- URL <http://www.scopus.com/inward/record.url?eid=2-s2.0-8491971148&partnerID=MN8TOAR&https://linkinghub.elsevier.com/retrieve/pii/S0263822314003602&http://dx.doi.org/10.1016/j.compstruct.2014.07.037>
- [50] S. G. P. Castro, Ritz method for the analysis of unstiffened laminated composite cylinders and cones under axial compression, in: *54th Israel Annual Conference on Aerospace Sciences 2014*, Vol. 2, 2014, pp. 1285–1302.
- [51] T. Rahman, E. Jansen, Finite Element Based Multi-Mode Initial Post-Buckling Analysis of Composite Cylindrical Shells, in: *50th AIAA/ASME/ASCE/AHS/ASC Structures, Structural Dynamics, and Materials Conference*, no. May, American Institute of Aeronautics and Astronautics, Palm Springs, California, 2009, pp. 4–7. doi:10.2514/6.2009-2557.
- URL <http://arc.aiaa.org/doi/10.2514/6.2009-2557>
- [52] S. G. P. Castro, Semi-analytical tools for the analysis of laminated composite cylindrical and conical imperfect shells under various loading and boundary conditions, Ph.D. thesis, Technische Universität Clausthal (2014).
- [53] L. Donnell, Stability of Thin-walled Tubes under Torsion, *Tech. Rep. 479*, NACA Report No. 479 (1933).
- [54] L. H. Donnell, A new theory for the buckling of thin cylinders under axial compression and bending, *Trans. ASME* 56 (11) (1934) 795–806.
- [55] A. N. Guz', G. V. Guz', Mechanics of composite materials with large-scale curving of filler (1983). doi:10.1007/BF00611782.
- [56] E. Burman, M. G. Larson, P. Hansbo, Cut Bogner-Fox-Schmit Elements for Plates (nov 2019). arXiv:1911.00239.
- URL <http://arxiv.org/abs/1911.00239>
- [57] J. H. Argyris, I. Fried, D. W. Scharpf, The TUBA Family of Plate Elements for the Matrix Displacement Method, *The Aeronautical Journal* 72 (692) (1968) 701–709. doi:10.1017/S000192400008489X.
- URL https://www.cambridge.org/core/product/identifier/S000192400008489X/type/journal_{_}article
- [58] O. O. Ochoa, J. N. Reddy, *Finite Element Analysis of Composite Laminates*, Springer, Dordrecht, 1992, pp. 37–109. doi:10.1007/978-94-015-7995-7_3.
- URL http://link.springer.com/10.1007/978-94-015-7995-7_{_}3
- [59] D. Q. Tsunematsu, The aeroelastic behavior of laminated composite panels undergoing progressive damage in supersonic flow, Thesis of doctor of science, Instituto Tecnológico de Aeronáutica (2019).
- [60] D. Q. Tsunematsu, M. V. Donadon, Aeroelastic behavior of composite panels undergoing progressive damage, *Composite Structures* 210 (2019) 458–472. doi:10.1016/J.COMPSTRUCT.2018.11.065.
- URL <https://www.sciencedirect.com/science/article/pii/S0263822318314508#b0110>
- [61] G. Van Rossum, F. L. Drake, *Python 3 Reference Manual*, CreateSpace, Scotts Valley, CA, 2009.
- [62] S. van der Walt, S. C. Colbert, G. Varoquaux, The NumPy Array: A Structure for Efficient Numerical Computation, *Computing in Science & Engineering* 13 (2) (2011) 22–30. arXiv:1102.1523, doi:10.1109/MCSE.2011.37.
- URL <http://ieeexplore.ieee.org/document/5725236/>
- [63] S. Behnel, R. Bradshaw, C. Citro, L. Dalcin, D. S. Seljebotn, K. Smith, Cython: The best of both worlds, *Computing in Science and Engineering* (2011). doi:10.1109/MCSE.2010.118.
- [64] A. D. Lanzo, G. Garcea, R. Casciaro, Asymptotic post-buckling analysis of rectangular plates by HC finite elements, *International Journal for Numerical Methods in Engineering* (1995). doi:10.1002/nme.1620381403.
- [65] N. D. Phan, J. N. Reddy, Analysis of laminated composite plates using a higher-order shear deformation theory, *International Journal for Numerical Methods in Engineering* 21 (12) (1985) 2201–2219. doi:10.1002/nme.1620211207.
- [66] A. Bilotta, A. D. Lanzo, R. Casciaro, A finite element for the koiter nonlinear analysis of composite thin-walled structures, in: *European Congress on Computational Methods in Applied Sciences and Engineering*, ECCOMAS, Barcelona, Espana, 2000.

- URL https://www.researchgate.net/publication/289009692_A_finite_element_for_the_koiter_nonlinear_analysis_of_composite_thin-walled_structures
- [67] E. L. Jansen, T. Rahman, Low-dimensional finite element based models for post-buckling and snap-through analysis of composite panels under dynamic in-plane loading, in: 6th Aircraft Structural Design Conference, Royal Aeronautical Society, Bristol, 2018.
- [68] J. Manie, DIANA 10.2 User's Manual (2017).
- [69] D. Allman, A compatible triangular element including vertex rotations for plane elasticity analysis, *Computers & Structures* 19 (1-2) (1984) 1–8. doi:[10.1016/0045-7949\(84\)90197-4](https://doi.org/10.1016/0045-7949(84)90197-4).
- URL <https://linkinghub.elsevier.com/retrieve/pii/0045794984901974>
- [70] D. J. Allman, Evaluation of the constant strain triangle with drilling rotations, *International Journal for Numerical Methods in Engineering* 26 (12) (1988) 2645–2655. doi:[10.1002/nme.1620261205](https://doi.wiley.com/10.1002/nme.1620261205)
- URL <http://doi.wiley.com/10.1002/nme.1620261205>
- [71] H. Jun, K. Yoon, P.-S. Lee, K.-J. Bathe, The MITC3+ shell element enriched in membrane displacements by interpolation covers, *Computer Methods in Applied Mechanics and Engineering* 337 (2018) 458–480. doi:[10.1016/j.cma.2018.04.007](https://doi.org/10.1016/j.cma.2018.04.007).
- URL <https://linkinghub.elsevier.com/retrieve/pii/S0045782518301774>
- [72] L. J. F. Ferreira, M. L. Bittencourt, Hierarchical high-order conforming C 1 bases for quadrangular and triangular finite elements, *International Journal for Numerical Methods in Engineering* 109 (7) (2017) 936–964. doi:[10.1002/nme.5308](https://doi.wiley.com/10.1002/nme.5308)
- URL <http://doi.wiley.com/10.1002/nme.5308>
- [73] S. G. Castro, T. A. Guimarães, D. A. Rade, M. V. Donadon, Flutter of stiffened composite panels considering the stiffener's base as a structural element, *Composite Structures* 140 (2016) 36–43. doi:[10.1016/j.compstruct.2015.12.056](https://doi.org/10.1016/j.compstruct.2015.12.056).
- URL <http://dx.doi.org/10.1016/j.compstruct.2015.12.056>
- [74] S. G. P. Castro, Computational mechanics tools (2016). doi:[10.5281/zenodo.2541512](https://doi.org/10.5281/zenodo.2541512)
- URL <https://doi.org/10.5281/zenodo.2541512>
- [75] S. G. Castro, M. V. Donadon, Assembly of semi-analytical models to address linear buckling and vibration of stiffened composite panels with debonding defect, *Composite Structures* 160 (2017) 232–247. doi:[10.1016/j.compstruct.2016.10.026](https://doi.org/10.1016/j.compstruct.2016.10.026).
- URL <http://linkinghub.elsevier.com/retrieve/pii/S026382231631008X>
- [76] S. G. P. Castro, Semi-analytical models for panels (jan 2020). doi:[10.5281/ZENODO.2541522](https://doi.org/10.5281/ZENODO.2541522).
- URL <https://doi.org/10.5281/zenodo.2541522>
- [77] H. Abramovich (Ed.), *Stability and Vibrations of Thin Walled Composite Structures*, 1st Edition, Woodhead Publishing, Haifa, Israel, 2017.
- URL <https://www.sciencedirect.com/book/9780081004104/stability-and-vibrations-of-thin-walled-composite-structures#book-description>
- [78] O. D. de Matos Junior, M. V. Donadon, S. G. Castro, Aeroelastic behavior of stiffened composite laminated panel with embedded SMA wire using the hierarchical Rayleigh–Ritz method, *Composite Structures* 181 (2017) 26–45. doi:[10.1016/j.compstruct.2017.08.060](https://doi.org/10.1016/j.compstruct.2017.08.060).
- URL <https://linkinghub.elsevier.com/retrieve/pii/S0263822317311807>
- [79] R. Vescovini, L. Dozio, M. D'Ottavio, O. Polit, On the application of the Ritz method to free vibration and buckling analysis of highly anisotropic plates, *Composite Structures* 192 (2018) 460–474. doi:[10.1016/j.compstruct.2018.03.017](https://doi.org/10.1016/j.compstruct.2018.03.017).
- URL <https://www.sciencedirect.com/science/article/pii/S0263822318305233#f0030>
- [80] R. Vescovini, E. Spigarolo, E. Jansen, L. Dozio, Efficient post-buckling analysis of variable-stiffness plates using a perturbation approach, *Thin-Walled Structures* 143 (2019) 106211. doi:[10.1016/j.tws.2019.106211](https://doi.org/10.1016/j.tws.2019.106211).